DS

NATIONAL RADIO ASTRONOMY OBSERVATORY
Green Bank, West Virginia

Electronics Division Internal Report No. 78

A CONTINUOUSLY RECORDING INFRARED HYGROMETER, AND RESULTS OF AN INTERFEROMETER-HYGROMETER CORRELATION EXPERIMENT

K. H. Wesseling

AUGUST 1968

NUMBER OF COPIES: 100

A CONTINUOUSLY RECORDING INFRARED HYGROMETER, AND RESULTS OF AN INTERFEROMETER-HYGROMETER CORRELATION EXPERIMENT

Karel H. Wesseling

ACKNOWLEDGMENT

It is a pleasure to thank the following people for their interest and help at various stages of the hygrometer project.

D. E. Hogg originally suggested the project. L. Beale has been cooperative in the mechanical design of the prototype hygrometer and was responsible for the production of five more instruments of a slightly modified design. J. Davis designed and produced a printed circuit board for the amplifier section and helped with the initial setup and measurements. J. P. Basart has been responsible for the execution of the interferometer-hygrometer correlation experiments. Together with Jo Ann Kramer he also did the computer programming that produced the diagrams of Figures 21, 23 and 24. S. Malott has given substantial help in later stages of programming and data reduction. Many discussions with W. J. Altenhoff, J. P. Basart, D. E. Hogg, and J. Schraml have helped in understanding the instrument and the method.

In conclusion, it is a special pleasure to mention the long, exhaustive and fruitful discussions with L. E. Snyder that raised questions and produced answers in most areas, particularly in molecular absorption and scatter effects of the atmosphere.

TABLE OF CONTENTS

LIST OF FIGURES

A CONTINUOUSLY RECORDING INFRARED HYGROMETER, AND RESULTS OF AN INTERFEROMETER-HYGROMETER CORRELATION EXPERIMENT

SUMMARY

In this report a continuously recording hygrometer is described together with its calibration procedure, first observations and the results of an experiment to correlate water vapor fluctuations measured with the hygrometer with instabilities observed in the output phase of an 11 cm wavelength interferometer.

The design of the hygrometer follows a method suggested by F. E. Fowle in 1912 (Ref. 5). Modifications as given by Foster, Voltz and Foskett (Ref. 4, 1963) and Low and Davidson (Ref. 9, 1965) are incorporated in the present instrument. This new instrument differs from the design by Low and Davidson in that it is automatic and continuously recording.

The instrument's calibration curve, obtained by performing dawn-to-dusk observations on several days of quiet atmospheric conditions, is checked against a similar curve obtained by Foster, et al., and against theory.

Further confirmation of the calibration curve has been obtained by comparing hygrometer readings of water vapor with phase fluctuation measurements obtained with an 11 cm wavelength interferometer. Correlations are judged significant, leading to two conclusions:

1) Interferometer phase fluctuations, under the meteorological conditions in existence at the time of the data acquisition, and for intermediate baseline lengths (order of 1 km), are largely caused by water vapor fluctuations in the field of view of the telescopes; and
2) Infrared hygrometers can be successfully used to predict interferometer phase fluctuation levels due to water vapor variations on clear days, to obtain a confidence check on whether interferometer indicated phase variations are due to source structure, or for the evaluation of future sites for interferometers with regard to water vapor.

1. INTRODUCTION

Early observations with the NRAO two-element interferometer of the amplitude and phase of radio point sources at 11 cm wavelength showed considerable instabilities, especially in the phase of the radio source. The fluctuations could not be ascribed to the astronomical object, it being a point source and of sufficiently large flux density (calibrator source). The observed phase fluctuations were big enough to cause considerable sidelobes during a significant part of the yearly observing time, if super synthesis operation of the interferometer were to be considered. In addition, the precise measurement of source positions would require very considerable integration times, to average out the large phase (hence apparent source position) fluctuations.

With the instrumentation available for the interferometer at the time, it was impossible to separate phase errors caused by irregular propagation effects in the atmosphere from instrumental phase instabilities. A significant correlation between rms phase errors and weather type, in particular the presence or absence of frontal activity, was nevertheless found by Baars (Ref. 1). Further investigation by Waters (Ref. 15) showed water vapor fluctuations in the troposphere to be a potentially large contributor to the observed phase fluctuations.

Clearly, further experiments were needed, and were made practical when the improved, now three-element, interferometer was inaugurated in June 1967. The new instrumentation for this interferometer features, among other things, a phase-stable local oscillator system (Ref. 17) reducing instrumental phase effects to slow diurnal drifts with a worst case peak-to-peak phase uncertainty of 5° (Ref. 16). With this kind of instrumental phase stability it is possible to ascribe calibrator apparent phase fluctuations to disturbances in the propagation path of the EM-waves through the earth's atmosphere only.

At about the same time (mid-1967) a continuously recording, infrared hygrometer, developed by the author, became operational and it was decided to correlate water vapor fluctuations as measured by the hygrometers with the residual fluctuations in the output phase of the interferometer, while observing a point source.

This report describes the hygrometer and how it is calibrated. Subsequent sections give the first results obtained with the hygrometer itself and the outcome of experiments, designed to investigate the correlation between interferometer phase

fluctuations and synchronous hygrometer water vapor measurements. Conclusions and suggestions for further work, where applicable, are given at the end of each section.

2. DESCRIPTION OF THE HYGROMETER

2.1 Introduction

A moderately absorbing water vapor band exists in the Sun's spectrum around 9350 Å, as spectroscopy observations have shown. The shape of this band is rather peculiar and is determined by the cumulative absorption of a large number of pressure broadened lines, from about six vibration-rotation groups. The absorption is moderate in that it does not give complete absorption under all normal circumstances encountered in the atmosphere. The depth of this absorption band then is a measure for the total amount of water vapor in the path, provided that vertical water vapor, pressure and temperature distributions are sufficiently well known or constant. This condition is not fulfilled, but the scatter (± 25%) in the observations is small enough to make the method usable.[1] The depth of the water vapor band is measured by comparing the level of radiation from the Sun at 9350 Å with that at 8800 Å, a wavelength virtually undisturbed by water vapor or other absorption lines. The ratio of the IR light levels at the two wavelengths determines the amount of water vapor in the line of sight.

2.2 Design of the Instrument

In the instrument under consideration the output of a photo detector at either 9350 or 8800 Å wavelength is amplified utilizing a variable gain DC amplifier. The gain at both wavelengths is equal, but is continuously adjusted to give a constant output level for the 8800 Å observation by means of a servo loop. In this case the 9350 Å output is a constant times the 9350/8800 ratio, which is the quantity proportional to the amount of absorbing water vapor.

---

[1] See Appendix A.

A block diagram of the instrument is given in Figure 1. A filter wheel rotates at 3000 rpm (50 Hz) in front of a photo detector. Two interference filters, one tuned at 8800 Å, the other at 9350 Å, are mounted in the wheel. Each filter has a half power bandwidth of 100 Å. The wheel also has one radial slot in the edge, for the synchronization of the sample and hold amplifiers shown later in the block diagram. The filter wheel is made out of aluminum and is carefully balanced. It rotates virtually vibration free and noiseless. The dimensions are given in Figure 2. A Hurst model 9 A 600 AC motor drives the wheel via pulleys and a rubber belt. Reduction in the drive train is 5: 6.

Typical for interference filters is the change in the passband characteristics for light incident at angles other than 90° or normal. For the filters at hand, the manufacturer (Thin Film Products, Inc.) states a shift of 20 Å in center wavelength towards longer wavelengths, for angles of incidence 5° from normal. This limits the beamwidth of the instrument to something less than 5°, because a shift of 20 Å causes a hygrometer output error of the order of 5%, as was found empirically. The temperature sensitivity of the filters is small. The filter's center wavelength shifts ± 5 Å for temperature changes of ± 20 °C.

The light sensor is a Texas Instruments type LS-400 silicon phototransistor. It is of the photoconductor type and can be considered a light controlled current source when series connected to a constant DC voltage source. It features good sensitivity, high speed of response, and a spectral response characteristic which peaks at 9000 Å. Its temperature sensitivity is negligible for the application at hand. The light intensity versus output current law of the detector is linear on a log-log scale. This characteristic makes it possible to give a calibration curve for the instrument, without reference to the actual light level. Figure 3 and Reference 12 give some pertinent LS-400 data.

The controlled gain operational amplifier following the photodetector converts the detector output current into a voltage. The conversion factor (in ohms) is electronically variable by varying the op amp's feedback resistor. The gain is set at a value giving a constant output voltage of -7 V DC during the period when the 8800 Å filter is in front of the photodetector. This value is maintained during the immediately following period when the 9350 Å filter is in this position. One complete revolution of the filter wheel takes place in 20 ms.

Two synchronous sample and hold amplifiers are connected in parallel to the variable gain amplifier output. Each of the two synchronous sample and hold amplifiers consists of a synchronous switch, a hold capacitor and a very high input impedance (10^{10} ohm), unity gain voltage follower using an operational amplifier, with an FET input stage. The synchronous switches are LS-400 photo conductors. A DC operated incandescent lamp located near each one of the LS-400 choppers illuminates the photo conductor for a short period of time (1/60 of a revolution or 1/3 ms) when the slot in the filter wheel allows the lamp to illuminate the LS-400. In this interval the LS-400 impedance is low and the input amplifier charges the hold capacitor to its output voltage with a time constant of a few milliseconds. During the rest of the time the LS-400 impedance is high and the capacitor holds its charge. The unity gain voltage follower performs the function of impedance converter. The position of the slot in the filter wheel is such that when the 8800 Å filter is intercepting the IR radiation to the detector, the 8800 synchronous switch is operated, and vice versa (see the timing diagram of Figure 1).

The output voltage of the 8800 synchronous S/H amplifier is compared with a stabilized DC voltage from a temperature-compensated zener diode. The difference is amplified and changes the gain of the variable gain input amplifier in such a way as to reduce the difference between the two inputs. A Raytheon Raysistor, type CK 1116, is utilized to close the servo loop. The percentage resistance change of the Raysistor is almost linearly proportional to the control current change and independent of the actual resistance value (or bias). This means that the open loop gain is almost constant, independent of the servo position. This feature greatly simplifies stabilization of the servo loop and guarantees an almost constant closed loop response time. Raysistor response to a control current change is rather slow (tens of milliseconds), and the rather complicated feedback network around the ALC loop amplifier is designed to decrease the loop response time. The servo loop is first order integrating.

The output of the 9350 S/H amplifier is the output of the instrument. In addition to this, both the 8800 level and the servo loop position can be monitored to check on proper instrument operation. All outputs are short-circuit proof. The instrument is completely self-contained and requires only 117 V, 60 Hz AC power. It operates within specifications at ambient temperatures of up to 50 °C. A detailed electronics circuit diagram is given in Figure 4.

2.3 The Completed Instrument

Six of these instruments have been built, at a component cost of $600 each. One instrument was a prototype and differs slightly in appearance from the other five. Differences, however, are minor and do not appreciably affect operation and calibration.

Figure 5 shows one hygrometer mounted on an Edmund Scientific equatorial mount (clock drive, heavy duty - $100).

Figure 6 shows the interior of a production type hygrometer. Filter wheel and synchronous switches are in the left-hand compartment. The narrow, middle compartment contains the belt drive and the LS-400 light sensor mounted in a metal sphere (eyeball) which facilitates the aiming of the photo detector at the input diaphragm. The right-hand compartment contains the electronics printed circuit board, the synchronous drive motor and starting capacitor, and the Nexus NPS-2, ± 15 V, 150 mA regulated power supply. AC line voltage and signal voltages connect via separate waterproof Bendix Pygmee connectors at the far right in the picture. The instrument housing is made from rectangular pieces of 1/4" aluminum plate. The construction is simple and rugged, but heavy.

3. CALIBRATION OF THE INSTRUMENT

3.1 Introduction

Previous ways of calibrating an IR hygrometer included flying the instrument in a U-2 aircraft above the troposphere to establish the instrument's zero point and the use of radiosondes to get an independent measurement of the total amount of water vapor. In addition to the inherent inaccuracies of IR hygrometry, both mentioned methods are of limited accuracy themselves, and introduce quite considerable additional errors.

It will be shown in the following that a trustworthy calibration curve can be obtained in a simpler way using known instrumental characteristics to establish the zero-point and a series of day-long observations during quiet atmospheric conditions to obtain the other points on the curve.

3.2 Finding the Zero Water Vapor Point

If no water vapor is assumed to be present in the measurement path, the hygrometer output can be computed from

the Sun's spectrum,

interference filter passbands,

light sensor spectral sensitivity, and

light sensor detector law.

The Sun's Spectrum: Because of the narrowness of the filter passbands (100 Å) it is sufficiently accurate to take the ratio of the Sun's intensities at the spot wavelengths of 9350 and 8800 Å. This ratio is approximately 0.9 and subject to uncertainties in the spectrum at sea level due to dry air absorption and selective scattering.

Interference Filter Passbands: The integrated transmissivity of the filters (area under the passband curves) is computed for each of the filters. Passband curves are individually measured by the manufacturer (Thin Film Products, Inc.) and manually integrated using a planimeter. The average 9350 to 8800 Å ratio for the six filter pairs is 0.79. All ratios lie between 0.78 and 0.80.

Light Sensor Spectral Sensitivity: The LS-400 spectral response curve is given by the manufacturer (Texas Instruments); see Figure 3. From it we find a 9350 to 8800 Å sensitivity ratio of 0.97. The first three factors taken together give a zero water vapor IR light intensity ratio of $0.9 \times 0.79 \times 0.97 \cong 0.7$.

Light Sensor Detector Law: This curve is also given by the manufacturer. If the photo current is I and irradiance is H, the relationship is

$$\log H = 0.73 \log I$$

Application of this relationship gives for the ordinate of the instrument's zero water vapor point a ratio of 0.62. (See Figures 7, 8, 9, and 10.)

3.3 Finding the Calibration Curve

Recordings of the hygrometer output have been made during four clear days in 1967. The recordings begin when the Sun rises from behind the mountains at Green Bank, W. Va. and end when the Sun sets in the evening. At the beginning and

at the end of the recording a high amount of water vapor is indicated, while a minimum is measured at the Sun's meridian crossing around 12 o'clock noon. Assuming a constant amount of water vapor during the day, the ratio of measured water vapor at each moment compared to that at meridian crossing is known, because it will increase with increasing zenith angle following the sec Z law. Also, at each moment, the hygrometer output is recorded. Plotting the data points as found this way on double log paper (see Figure 7), delivers a curve of fixed shape but of unknown position on the horizontal or water vapor axis. By following this routine for several days, and shifting the curves in the horizontal direction until they match, a smooth curve can be drawn through the data points and the zero water vapor point and a calibration curve is obtained.

The actual data points show quite some scatter and the calibration curve is a best fit to the data points. The curve is shown in Figures 7, 8, 9 and 10. Table I gives numerical values for points on the curve.

3.4 Comparison with the U. S. Weather Bureau Calibration Curve

The U. S. Weather Bureau has built a similar instrument[2] (but with slightly different filters and a different kind of light sensor) and published a calibration curve for it. This curve was derived from data taken in Tucson, Arizona, which is at almost the same elevation as Green Bank, W. Va. The U. S. Weather Bureau curve is plotted in Figure 11, together with the curve obtained at NRAO-Green Bank. The two curves match rather well, if the Green Bank curve is adapted for a difference in detector laws, as is shown in Figure 11 (dashed curve). The exponent used in the conversion formula was 0.435, i.e., log (Ratio at USWB) = 0.435 log (Ratio at NRAO).

3.5 Intercomparison Between Two Hygrometers

The data on which the calibration curve is based was taken with one hygrometer. The critical component in the hygrometer on which the calibration depends is the LS-400 photo detector light current versus irradiance curve.

---

[2] See Foster, Foltz and Foskett (1964), Ref. 4.

A laboratory intercomparison test using an incandescent lamp as the light source gave a ratio reading of 0.78 average, all ratios being between 0.75 and 0.81. A preliminary test with two hygrometers spaced one meter apart and both tracking the Sun gave readings for the total water vapor of 47 and 51 mm at meridian crossing and the time fluctuations in each measurement agree extremely well. A 1.5-hour record on which the output of the two hygrometers is shown is reproduced in Figure 12.

3.6 Comparison with Theoretical Water Vapor Absorption Curves

The shape of the calibration curve of Figure 8 was somewhat surprising at first. A straight line, for example, as measured for liquid water (Figure 15) seemed more logical (Beer's law absorber). However, the shape of the water vapor calibration curve has been predicted theoretically under various and different assumptions by Elsasser, Goody, King and others (Ref. 13, Chapter 16). The Goody model absorption, which follows the empirical curve rather closely, assumes Lorentz-shaped lines randomly distributed in wave number and exponentially distributed in intensity and with constant line half-widths. These assumptions fit the absorption line measurements for water vapor reasonably well (see Ref. 2). Goody then calculates the transmission function for this model, taking the various molecular interactions into account. The transmission function thus found compares in a qualitative way with the empirical hygrometer calibration curve; see Figure 10.

3.7 Conclusion and Future Work

The calibration curve for the new hygrometer as derived in the previous sections agrees reasonably well with the one derived by the USWB and follows in a qualitative sense the theoretical predictions for a Goody model absorption band.

The data on which the calibration curve is based was taken with one hygrometer, and only four days worth of data was used in the derivation. The water vapor content on these days was rather high, and the calibration curves found for each day show an appreciable amount of scatter among each other. It is therefore desirable to get some more full day runs, especially also on winter days, with small amounts of precipitable water vapor. Information in this region is missing in the present evaluation.

Also, all six hygrometers should be intercompared, while sampling essentially the same path.

A future theoretical verification of the hygrometer calibration curve will assume an absorption band model that most closely fits the known water vapor absorption lines in the spectral region of interest. Also, various water vapor distributions with altitude, and thus with pressure and temperature will be assumed. Under these assumptions it should be possible to theoretically reproduce the empirical curve and the scatter area, representing the various meteorological conditions and water vapor distributions, in a quantitative manner.

It should be emphasized again that although a unique calibration curve is given, this curve actually is a "best fit" to observed data points which show a rather large scatter. A scatter of ± 25% in the indicated water vapor was found by the USWB. The scatter area is depicted in Figure 13.

4. FIRST OBSERVATIONS AND AN INSTRUMENTAL LIMITATION

4.1 Records Used to Obtain the Calibration Curve

Figure 14 gives records taken on the 25th and 26th of September and the 3rd of October, 1967, in Green Bank, W. Va. (elevation 800 m). These records and one taken on the 4th of October were used in finding the calibration curve. The records shown in Figure 14 are cut into two at meridian crossing. The amount of water vapor decreases (with air mass) towards meridian crossing and increases again towards sunset.

Note the steps in the record, when the tracking of the instrument was corrected. The jumps are caused by the change in the angle of incidence of the radiation upon the interference filter giving a filter passband shift and hence a different ratio reading. (See Section 2.2.) Also note the cloud passages through the beam at various instances. Clouds produce a more pronounced effect on the indicated amount of water vapor than is to be expected from other cloud water vapor measurements, and this effect needs further investigation.

4.2 The Effects of Clouds

A record showing cloud passages more clearly is given in Figure 15. It was taken on September 27, 1967, in Green Bank. In the figure, mention is made of other pertinent meteorological information.

Although the water vapor density inside clouds is indeed higher than outside the cloud (essentially saturated vapor), the increase in actual water vapor is by no means as great as suggested by the record. It should be mentioned here that the instrument was operating correctly, i.e., light levels were high enough to produce a constant 8800 Å reference -7 V DC at all times. A number of reasons can be thought of to explain the effect qualitatively, and are given in the following:

(a) A change in the light sensor detector law at low light levels. This hypothesis is not confirmed by the detector law as given by the manufacturer of the light sensors. (Refer to Figure 3.)

(b) Wavelength dependent extinction due to scatter in clouds. A reference to this effect is found in Carrier, et al. (Ref. 3). The extinction results mentioned in this reference are summarized in Table II of this report. Representative cloud drop size distributions and concentrations have been taken into account in the calculation of these numbers. Spherical water droplets have been assumed and the exact Mie theory (Ref. 6) has been used in the calculations. The facts relevant to this problem are that single scattering extinction is virtually constant with wavelength for each particular cloud model and secondly that optical extinction is strongly variable with cloud type with up to almost an order of magnitude differences. It should be noted that the refractive index for calculations at the three shortest wavelengths in this table has been taken as 1.38, without an imaginary part, i.e., no absorption has been taken into account.

(c) Absorption in liquid water. Yamatera, et al. (Ref. 18) show the existence of a weak liquid water absorption line at approximately 9700 Å, with the tail extending into the 9350 Å region. The absorption is dependent on temperature, the 9350 Å absorption becoming smaller with lower temperatures. No absorption line exists for ice at this wavelength. A laboratory experiment was arranged to measure the liquid water absorption. The hygrometer was put in a vertical position looking upwards. A glass container was placed over the aperture, and an incandescent lamp fed by a regulated DC power supply mounted above the container. Water was poured into the container and the change in hygrometer output

recorded. A calibration curve for liquid water absorption was thus obtained, and is given in Figure 16. Scatter in the measurements was smaller than ± 0.25 mm of liquid water. The curve is a straight line on semilog paper, which is to be expected for a simple absorber. The zero liquid water point in Figure 16 is dependent on the color temperature of the lamp, and no significance is to be attached to the 0.8 ratio as this will be the same 0.62 ratio as for water vapor when measured using sunlight.

Figure 16 indicates a liquid water absorption at 9350 Å which is much smaller than that of water vapor if equal amounts are taken, expressed in precipitable cm's. This is mainly because 9350 Å lies in the tail of the liquid water absorption band. Actual clouds contain to within an order of magnitude equal amounts of liquid water and water vapor, while the amount of water vapor (in g/m^3) is usually predominant. For these two reasons (equal amounts of water and water vapor, but water vapor a more effective absorber) it is concluded that liquid water absorption, although present, cannot explain the large increase in measured absorption at moments when a cloud moves in between the Sun and the hygrometer. Note: Clouds contain liquid water in the form of droplets, and it is assumed here that water droplets give the same selective absorption as an equal amount of water precipitated in a homogeneous layer. Calculations made in Appendix B seem to indicate that this is nearly true.

(d) The multiple traverse cell effect due to multiple scattering.

Van de Hulst (Ref. 6) gives a criterion for the occurrence of multiple scattering in terms of optical depth. For optically thin clouds with $\tau < 0.1$ (extinction less than 10%) single scattering prevails. For $0.1 < \tau < 0.3$ (extinction between 10 and 25%) corrections for double scattering should be made. Finally, for $\tau > 0.3$ (extinction more than 25%) the effects of multiple scattering have to be taken into account. If multiple scattering occurs, the effective pathlength through the absorbing medium increases (although equally much at 8800 and 9350 Å). An increased pathlength means increased absorption at 9350 Å and thus an apparent increase in precipitable water vapor. The increase in effective pathlength due to multiple scatter in a cloud as given by Kattawar, et al. (Ref. 8) is big enough to account for the observations.

In conclusion, of the four possible effects to explain the observed strong increase in absorption in clouds: the light sensor detector law, wavelength dependent scatter, liquid water absorption and effective pathlength increase; only the last one is large enough to explain the observations. Liquid water absorption is a less important but definitely contributing factor.

4.3 Fluctuations on a Turbulent Day

The record as reproduced in Figure 17 was taken on the roof of the NRAO building in Charlottesville, Virginia (elevation $\sim$ 170 m). It represents the water vapor fluctuations in the line of sight from the hygrometer to the Sun, for two hours on July 1, 1968. July 1 was a clear, hot day with winds 10 to 15 miles per hour, and the relative humidity approximately 40%. The next day there were thunderstorms with hail and heavy rain from about 12:00 noon until about 12:00 midnight.

The left trace shows total precipitable water vapor. Precipitable water vapor was a high 35 mm per unit air mass and dropped to an average 25 mm on July 3, the day after the thunderstorm.

The right trace shows with 5 times higher sensitivity the water vapor fluctuations with time. This trace was obtained by removing the DC term from the hygrometer output by means of a CR-differentiating network with a time constant of 2400 seconds. Water vapor fluctuations are big and fast.

Three out of several remarkable cases are sketched on the left of the record. The first one shows a variation of 2.7 mm of water vapor in 4.5 minutes, corresponding to 0.6 mm/min. The second and the third case both have approximately 0.4 mm/min variation. Much small scale structure can also be seen, particularly in the right-hand high sensitivity trace. The instrumental noise has been measured and is about 0.5 mV RMS, corresponding (see calibration curve) to 0.02 mm water vapor at the 1 V (35 mm water vapor) level and 0.05 mm water vapor at the 0.5 V (or 70 mm water vapor) level. Therefore, the small scale structure with amplitudes bigger than $\sim$1 minor division on the chart represents real changes in water vapor.

At this point the shape of the beam of the hygrometer should be examined in order to estimate what size structure in the water vapor field is discernable with the instrument. Figure 18 gives the beam shape versus height of the hygrometer, when looking almost vertically upwards. At the right in the same diagram is shown the approximate yearly average water vapor distribution with height. The diameter of the hygrometer beam for small zenith distances is less than 25 m at altitudes below 2 km. Fifty percent of all the water vapor in the average is below 2 km. A beam of this size permits the observation of water vapor blobs of sizes as small as 50 m, virtually unattenuated by beam-smoothing effects.

At a wind speed of 10 m/s and the water vapor distribution field constant with regard to a coordinate system moving with the wind, it takes 5 seconds for a 50 m big water vapor concentration blob to pass through the beam. Water vapor fluctuations with periods of this order indeed appear to be present on the record with amplitudes considerably bigger than the noise. Many of the bigger water vapor fluctuations last "typically" 300 seconds. Assuming the same 10 m/s wind speed, the size of these blobs is 3 km, giving an approximate correlation distance of 750 m.

5. INTERFEROMETER-HYGROMETER CORRELATIONS

5.1 Introduction

Earthbound interferometric observations of radio sources at cm wavelengths and with interferometer baselines of the order of 1 km or longer are significantly disturbed by changes in the refractive index of the air. Several agents are known to cause changes in the refractive index of the atmosphere at cm and dm wavelengths, notably the ionosphere, dry air pressure and temperature effects, water vapor, and liquid water in clouds and rain.

(a) The ionosphere. Mathur (Ref. 10) calculated the effect of the ionosphere for various interferometer baseline lengths at a wavelength of 11 cm and concluded that ionospheric effects are negligible compared to errors introduced by the troposphere, except under highly disturbed ionospheric conditions. Then they can be as much as the tropospheric errors.

(b) Dry air pressure and temperature changes. Of the two, the pressure variations are small and have a very large horizontal scale and thus should not be a disturbing factor. With regard to temperature variations, a dry air temperature variation of 10 °C extending vertically over the lower 3 km of the atmosphere causes a phase error of approximately 20° at 11 cm wavelength. Reference 13 gives ground level temperature variations and scale sizes under a number of meteorological conditions. This information is reproduced in Table III. It can be concluded that dry air temperature variations can have a significant effect on the interferometer phase for baselines of more than a few kilometers.

(c) Water vapor fluctuations. J. Waters (Ref. 15) has calculated the effect of a change in the amount of water vapor on the interferometer phase at 11 cm wavelength. At this wavelength the conversion factor is 200 degrees phase retardation per cm precipitable water in the propagation path in the form of water vapor. The conversion factor is temperature dependent but is accurate to 5 or 10% under most conditions. It has already been shown (Figure 17) that fluctuations as much as 3 mm of precipitable water may occur over time spans of only a few minutes, corresponding to a 60° change in phase delay in one arm of an interferometer. Long-term water vapor fluctuations can be even bigger than this — a substantial part of the scatter in the calibration curve, it is believed, is caused by these long-term (daily) fluctuations — but have time scales of the order of hours. Such long-term fluctuations can be calibrated and subtracted from the interferometer measurements by observing "calibrators". Calibrators are radio sources of very small size and of known or assumed position in the sky. Short-term water vapor fluctuations (with time spans less than 1 minute) are usually small, which is due in part to the integrating effect of the telescope beam cross section. The residual effect will be averaged out in the receiver's time constant, or at the worse cause a small reduction in apparent source flux.

It is the intermediate term phase fluctuations with up to one hour time scales that are of the greatest concern in interferometric radio astronomy observations. They change too quickly to be calibrated out and in addition disturb the long-term fluctuation calibration so that a large percentage of the observing time has to be spent on calibrators.

(d) Liquid water in clouds and rain. Liquid water droplets of sizes much smaller than the wavelength couple inefficiently with the EM-wave and produce only small changes in effective dielectric constant. Meinke, et al. (Ref. 11) state: "If the total amount of water vapor in moist air would condense in the form of liquid water droplets, the part of the effective dielectric constant due to water would drop to 10% of its original value." However, an extremely wet cloud with 10 g/m^3 of liquid water, 1 km thick, contains 1 cm of precipitable water which will still cause 20° of phase retardation. Generally, large air motions and temperature gradients exist in clouds which also contribute to a change in the refractive index. Measured

deviations in the refractive index of clouds from the surrounding air, in N units, range from 0 to 20 as given in the Handbook of Geophysics (Ref. 13, Chapter 13). A 1 km thick cloud in one arm of the interferometer with a difference in the refractive index of 10 N units will cause a phase error of 30°.

Conclusion: Of the four possible factors to cause errors in the apparent interferometer phase of a radio source, the water vapor fluctuations seem to be the most probable disturbing agent on clear days for intermediate length (order of 1 km) baselines at 11 cm wavelength. It should, therefore, be possible to compare interferometer phase fluctuations on clear days with hygrometer readings and find a significant correlation. If such a correlation exists it is proven that tropospheric water vapor fluctuations are the main source of disturbance in interferometric observations under the conditions stated previously. At the same time a further check on the hygrometer calibration has been obtained, and hygrometer information can be used with confidence to evaluate sites for future interferometers, the hygrometers being inexpensive, easily portable, and simple to operate. In addition, a hygrometer can provide a validity check on radio source phase information as obtained from an interferometer on an almost instantaneous basis, by using the indicated water vapor fluctuation levels.

5.2 The NRAO Interferometer in Green Bank

Three 26 m (85 ft) radio telescopes and a receiver system form a variable baseline interferometer with a maximum baseline, or antenna separation, of 2700 m. It is operated by the NRAO in Green Bank, West Virginia. Site elevation is approximately 800 m. Three dishes are operated simultaneously at 11 cm wavelength. Instrumental phase errors are less than 5° p-p and have the form of slow diurnal drifts; see Ref. 16. The sensitivity of the receiver system is high enough to be able to observe a 10 flux unit radio source, with a signal-to-noise ratio of better than 25 to 1, producing phase variations due to noise of less than 2° RMS. Figure 19 gives an impression of the interferometer and the control building. In the same picture a 300 ft (grey) and a 140 ft (background—white) radio telescope are visible.

5.3 Experimental Setup

To measure hygrometer output versus interferometer phase correlation, a number of near-occultation experiments were scheduled with the interferometer as follows.

The interferometer tracks a radio point source of known position, preferably only a couple of degrees away from the Sun (near-occultation). A hygrometer is located near each one of the dishes of the interferometer and tracks the Sun (Figure 20). The phase of the interferometer output is constant (tracking interferometer) if no disturbing factors are present, and possible output fluctuations will at least in part be due to changes in water vapor difference distribution in the direction of the source, as sampled by each of the dishes. Each one of the hygrometers measures total precipitable water vapor in a 1/2° beam in its line of sight to the Sun. Subtraction of the two hygrometer outputs, after conversion to precipitable centimeters of water vapor, gives a measure for the differential water vapor distribution in its field of view. The areas sampled by an interferometer dish and its associated hygrometer have to be substantially the same and close enough together to observe essentially the same water vapor. Examination of Figure 18 shows that the paths over which the water vapor distribution is sampled by the interferometer against a point source and by the hygrometer against the Sun have no point in common. Assumed in Figure 18 is that the position of the point source is 2° away from the Sun. From this it follows that water vapor fluctuation of small scale sizes will be seen differently by the two instruments. However, the relative amplitude of these fluctuations will be small. Fluctuations of larger scale, although sampled at different points, possibly as far apart as 200 m, should have an almost identical effect on both the hygrometers and the interferometer. From this it follows, however, that 100% correlation cannot be expected, not even if time shifts are introduced in the cross-correlation computations.

5.4 Observations

Three days of near-occultation experiments were judged successful out of a total of almost ten scheduled, and the results obtained are given below. Observations on the remaining seven days failed for a variety of reasons, among them

cloudy weather (a major one), hygrometer malfunction (now cured), and computer breakdown (rare). (The entire interferometer operation is computer controlled and monitored, including hygrometer output data acquisition.)

October 12, 1967

Scan Numbers 9217-19

Radio Source 3C 279 — Flux: 12 units
RA: $12^h\ 54^m$
δ: -05° 37'

Interferometer Baseline: 1900 m

Sun - Source Separation: $\sim$ 2°

Comment:

Refer to Figure 21.

Plotted are: A = Source Amplitude.

P = Source Phase (0-360°) in 3° increments.

1 = Hygrometer No. 1 water vapor fluctuations converted to phase (0-360°) in 3° increments.

2 = id., Hygrometer No. 2.

H = 1-2 = id., hygrometer difference fluctuation.

One set of information points is plotted every minute of time.

Points of the H and P plots are interconnected with a solid line.

A dashed line indicates erroneous results, due to interference.

No particular significance is to be attached to the position of the plots on the phase scale, and zero points are to be considered arbitrary. A linear slope in the plots is also to be ignored, as this is most likely caused by small tracking errors in the hygrometers following the Sun, by deviations from the hygrometer calibration curve on a particular day and by small errors in the assumed radio source position.

Several interesting facts can be noted in the plots:

(a) The peak-to-peak fluctuation value of both the H and the P plots is about 30°. A point-to-point correspondence between H and P can be observed, as a rule, although

not consistently. Most times a time shift of 1 or 2 minutes between H and P is present. Generally, both the H and P fluctuations have the same rate of change and sense of direction over periods of minutes as well as hours.

(b) RMS fluctuations and cross-correlation coefficients ρ have been computed as follows. A sloped straight line was fitted to the data points of each scan in an RMS sense, and subsequently subtracted. H and P are now plotted again. The result for scans Nos. 9217 and 9256 are shown in Figure 22. RMS values and cross correlation are now computed, and given in table form.

Subtracting a straight line, which was fitted in an RMS sense, is not the correct mathematical procedure, because it might result in a DC offset. Resulting errors, however, are small, due to the rather symmetrical P and H amplitude distributions, and the RMS-fit was available in the program library.

The following table gives the computed values:

Scan Number	9217	9218	9219	Unit
P.....	7.0	*)	9.7	°RMS
H.....	10.5		6.6	°RMS
$\rho(-1)$.....	71		50	%
$\rho(0)$	54		23	%
$\rho(+1)$.....	41		0	%
Duration ...	1	1	1/2	hr

*) Values not computed because of bad section in input data.

It is possible that $\rho(-2)$ for scan 9219 would have shown an even higher percentage correlation, as inspection of the printout shows a relative shift of 2 units of time (2 min) in the most significant zero crossings. Note that H > P in scan 9217 and that the opposite is true in scan 9219. No explanation is offered.

(3) Although the total water vapor phase as measured with hygrometers 1 and 2 is subtracted to find the difference fluctuation H, the fluctuation in H is equal to the sum of the fluctuations in 1 and 2 in a statistical sense. This indicates essentially independent water vapor fluctuations at stations 1900 m apart, suggesting a spatial water vapor correlation distance of less than 1000 m, for the fluctuations under consideration.

October 13, 1967

Scan Numbers 9255-57

Radio Source Observed : The same as the previous

Interferometer Configuration: day.

Comment:

Refer to Figure 23.

Fluctuation levels are smaller this day that the day before. This is noticeable in both the H and the P plot.

RMS fluctuations and cross correlations have been computed again, and are given in the following table:

Scan Number	9255	9256	9257	Unit
P	2.8	3.9	5.6	°RMS
H	2.9	4.6	5.5	°RMS
$\rho(-1)$	31	68	57	%
$\rho(0)$	37	55	52	%
$\rho(+1)$	35	32	40	%
Duration..	1/2	1	1	hr

Correlation is expected to be less this day than on days with larger fluctuations, due to signal-to-noise ratio effects becoming more significant at the low RMS phase fluctuation levels encountered at this particular day.

January 19, 1968

Scan Numbers: 5284

Radio Source: 1938-15 — Flux: 4.0 units
RA: $19^h\ 39^m$
δ: -15° 29'

Interferometer Baseline: 2100 m

Sun-Source Separation: ~ 6°

Comment:

Refer to Figure 24.

Only one hygrometer, located at telescope 85-1, was used for this scan. No cross correlations were computed for this reason. Inspection of the record shows a remarkable H, P correlation during the first half hour with a time shift of one unit (1 min), the correlation becoming smaller and vanishing towards the second half of the record. It gives the impression of a water vapor fluctuation field of rather limited size moving over 85-1 telescope and hygrometer first; then this same field, or another field moving over 85-2

disturbing the phase, but not the hygrometer, no hygrometer being present to sample that field. During the entire scan the H fluctuation level is lower than the P fluctuation level, due to the missing contribution of the second hygrometer.

5.5 Conclusions and Future Work

Significant correlation (up to 70%) has been shown to exist between actual interferometer phase fluctuations and phase fluctuations predicted by IR hygrometer water vapor measurements on clear days.

The observed correlation is surprisingly strong in view of the many uncertainties and sources of inaccuracy in the comparison. To summarize:

a. The difference in shape of the interferometer and hygrometer beams (Figure 18).

b. The difference in direction of pointing of the beams, and the difference in position of corresponding instruments in the horizontal plane (Figure 18).

c. The uncertainty in the hygrometer calibration curve (Figure 13).

d. The uncertainty in the conversion from centimeters precipitable water vapor to degrees of phase shift at 11 cm wavelength (Reference 15).

e. Other causes of interferometer phase shift, not measured by IR hygrometers, such as dry air temperature changes, and the ionosphere (Section 5.1).

f. The possible effect of haze, which is strong on the hygrometer readings, and almost negligible on the interferometer phase (Sections 4.2 and 5.1).

g. The limited signal-to-noise ratios, both in the actual and the predicted phase.

A double conclusion can be drawn:

a) Intermediate term phase fluctuations in the interferometer output are, at least for a large percentage, caused by changes in the water vapor distribution, over baseline lengths of the order of 1 km.

b) Infrared hygrometers can be successfully used in predicting interferometer phase fluctuation levels of the type considered, on clear days. Hygrometers can thus, for example, be used on a continuous basis as a further check on the validity of observed interferometer output phase changes for radio sources that are not point sources and hence would show variations originating in the source itself.

Future work in this area of investigation should include near-occultation observations under all clear weather conditions, and should include small (less than 1 km) and very large (more than 10 km) phase stable baselines. Probability distributions for H, P, and hygrometer 1 and 2 outputs should be computed and evaluated, in addition to more complete auto- and cross-correlation functions for the H and P outputs. A cross-correlation analysis between hygrometer outputs 1 and 2 would give a further check on a previous statement (which was based on a visual inspection of the records) that no such correlation exists over the baseline lengths considered.

REFERENCES

1. J. W. M. Baars: "Meteorological Influences on Radio Interferometer Phase Fluctuations," IEEE Trans., AP-15, 582 (1967).

2. D. E. Burch, D. A. Gryvnak: "Absorption by H_2O between 5045-14,485 cm^{-1}," Aeronutronic Scientific Report Publication No. U-3704; AD 657629 (31 July 1966).

3. L. W. Carrier, G. A. Cato, K. T. von Essen: "The Backscattering and Extinction of Visible and Infrared Radiation by Selected Major Cloud Models," Applied Optics, 6, 1209 (1967).

4. N. B. Foster, D. T. Volz, L. W. Foskett: "A Spectral Hygrometer for Measuring Total Precipitable Water," Humidity and Moisture, Vol. I, New York: Reinhold Pub. Corp. (1964).

5. F. E. Fowle: "The Spectroscopic Determination of Aqueous Vapor," Ap. J., 35, 149-162 (1912).

6. H. C. van de Hulst: Light Scattering by Small Particles, John Wiley and Sons, Inc. (1957).

7. G. W. Kattawar, G. N. Plass: "Electromagnetic Scattering from Absorbing Spheres," Applied Optics, 6, 1377 (1967).

8. G. W. Kattawar, G. N. Plass: "Influence of Particle Size Distribution on Reflected and Transmitted Light from Clouds," AFCRL Report, Accession Number N67-37266 (1967).

9. F. Low, A. Davidson: "Measurement of Atmospheric Attenuation at 1 mm and a Description of a Portable Spectral Hygrometer," NRAO Internal Report (1965).

10. N. C. Mathur: "Ionospheric Effects at 11 cm Wavelength," VLA Scientific Memorandum No. 9 (1967).

11. H. Meinke, F. W. Gundlach: Taschenbuch der Hochfrequenztechnik, 2nd Edition (1962).

12. "Silicon Planar Photo Device LS-400," Texas Instruments Application Note.

13. USAF Handbook of Geophysics, 2nd Edition (1960).

14. U.S. Standard Atmosphere (1962).

15. J. W. Waters: "Atmospheric Effects on Radio Wave Phase, etc.," VLA Scientific Memorandum No. 8 (1967).

REFERENCES (CONTINUED):

16. K. H. Wesseling: "Gain and Phase Stability of the Interferometer as Determined by the LO System," Interferometer Group Memo No. 18 (1967).

17. K. H. Wesseling: "Interferometer Local Oscillator System Description," Interferometer Group Memo No. 19 (1967).

18. H. Yamatera, B. Fitzpatrick, G. Gordon: "Near Infrared Spectra of Water and Aqueous Solutions," J. of Molec. Spectroscopy, 14, 268-278 (1964).

APPENDIX A

The fractional absorption A, occurring in an atmospheric layer of finite thickness can be approximated in a formula as follows (Ref. 4):

$$A = \frac{k\sqrt{XP}}{\sqrt[4]{T}}$$

where A = fractional absorption

X = mass

P = pressure

T = absolute temperature

k = dimensional constant.

This expression is approximate in that the effect of pressure, in practice, is in between $\sqrt{P}$ and $\sqrt[4]{P}$, due to a multitude of overlapping absorption lines.

As the water vapor distribution with height changes from day to day, and the temperature changes significantly even during the day, the hygrometer output cannot be converted to amount of water vapor, unless the exact absorption formula and the water vapor, pressure and temperature distributions are known. Using U.S. standard atmosphere data (Ref. 14), a certain amount of water vapor at 1 km height would give about 3 percent more absorption than at 2 km, using the formula stated above with $\sqrt[3]{P}$ pressure dependence.

APPENDIX B

Using the results obtained by Kattawar (Ref. 7) for the absorption efficiency factor Q_{abs} for a complex dielectric constant m of

$$m = 1.33 - i\ 0.01$$

we find for the three values of x (particle size parameter) for which graphs are given:

$$x = 0.1 \qquad Q_{abs} = 2 \times 10^{-3}$$
$$= 1 \qquad = 3 \times 10^{-2}$$
$$= 10 \qquad = 3.7 \times 10^{-1}$$

The volume of the scattering particle can be calculated from

$$VOL = \frac{4}{3}\ \pi\ a^3 \qquad \text{with} \quad a = \text{radius of particle}$$
$$= \frac{x\lambda}{2\pi}$$

Assuming a constant wavelength $\lambda = 1\ \mu m$, we find for the volume of one particle expressed in x

$$VOL = \frac{x^3}{6\pi^2}$$

Assuming a constant amount of liquid water expressed in g/m^3 for the various x sizes, the number of scattering particles N is inversely proportional to the volume of each particle:

$$N \overset{\propto}{=} \frac{6\pi^2}{x^3}$$

The geometrical cross section of the water droplet is

$$G = \pi a^2 = \frac{x^2}{4\pi}$$

Assuming optically thin clouds with single scattering, each particle in a volume is equally effective (no shielding). The total absorption ABS is proportional to the number of scattering particles as computed above, and their scattering cross section $Q_{abs} \times G$ as follows:

$$ABS = N \times G \times Q_{abs}$$

$$= \frac{6\pi^2}{x^3} \cdot \frac{x^2}{4\pi} \quad Q_{abs} = \frac{6\pi}{4} \frac{1}{x}$$

For $x = 0.1$	$Q_{abs} = 2.1 \times 10^{-3}$	$ABS = 9.9 \times 10^{-2}$
$x = 1$	$Q_{abs} = 2.7 \times 10^{-2}$	$ABS = 13 \times 10^{-2}$
$x = 10$	$Q_{abs} = 3.6 \times 10^{-1}$	$ABS = 17 \times 10^{-2}$

It follows that the absorption of infrared radiation of 1 μm wavelength is only slightly dependent on particle size, for a constant amount of liquid water per unit of volume. The dependence is such that the absorption increases with increasing droplet size.

Laboratory measurement of the absorption of a layer of liquid water should thus provide an upper limit for the selective absorption of 9350 Å radiation by water droplets.

Water Vapor Ratio	Water Vapor cm	Water Vapor Volts	1st Diff. mV
0.62	0	4.340	1260
0.44	0.5	3.080	700
0.34	1.0	2.380	420
0.28	1.5	1.960	315
0.235	2.0	1.645	238
0.201	2.5	1.407	196
0.173	3.0	1.211	147
0.152	3.5	1.064	147
0.131	4.0	.917	105
0.116	4.5	.812	77
0.105	5.0	.735	77
0.094	5.5	.658	63
0.085	6.0	.595	49
0.078	6.5	.546	49
0.071	7.0	.497	42
0.065	7.5	.455	42
0.059	8.0	.413	35
0.054	8.5	.378	28
0.050	9.0	.350	28
0.046	9.5	.322	21
0.043	10.0	.301	---

TABLE I. HYGROMETER CALIBRATION CURVE

Cloud Type	Optical Extinction $b(m^{-1})$				
	Wavelength				
	0.488 μ	0.694 μ	1.06 μ	4.0 μ	10.6 μ
Nimbostratus	1.28×10^{-1}	1.30×10^{-1}	1.32×10^{-1}	1.47×10^{-1}	1.36×10^{-1}
Altostratus	1.08×10^{-1}	1.09×10^{-1}	1.12×10^{-1}	1.30×10^{-1}	8.39×10^{-2}
Stratus II	1.00×10^{-1}	1.01×10^{-1}	1.03×10^{-1}	1.14×10^{-1}	1.04×10^{-1}
Cumulus congestus	6.92×10^{-2}	6.98×10^{-2}	7.13×10^{-2}	8.10×10^{-2}	6.76×10^{-2}
Stratus I	6.69×10^{-2}	6.79×10^{-2}	6.97×10^{-2}	9.01×10^{-2}	4.28×10^{-2}
Cumulonimbus	4.35×10^{-2}	4.38×10^{-2}	4.44×10^{-2}	4.82×10^{-2}	5.09×10^{-2}
Stratocumulus	4.53×10^{-2}	4.60×10^{-2}	4.71×10^{-2}	5.96×10^{-2}	2.48×10^{-2}
Fair Wx cumulus	2.10×10^{-2}	2.13×10^{-2}	2.19×10^{-2}	2.76×10^{-2}	1.17×10^{-2}

TABLE II. SUMMARY OF THE EXTINCTION COEFFICIENTS OF THE MAJOR CLOUD TYPES

Local Condition	Horizontal Scale (mi)	ΔT (°F)
Difference in air mass ..	100-1000	5-40
Weather fronts	10-100	5-40
Squall lines	5-50	5-30
Thunder storms	5-15	5-30
Sea breeze	5-10	2-20
Land breeze	2-5	2-10

TABLE III. DRY AIR TEMPERATURE VARIATIONS

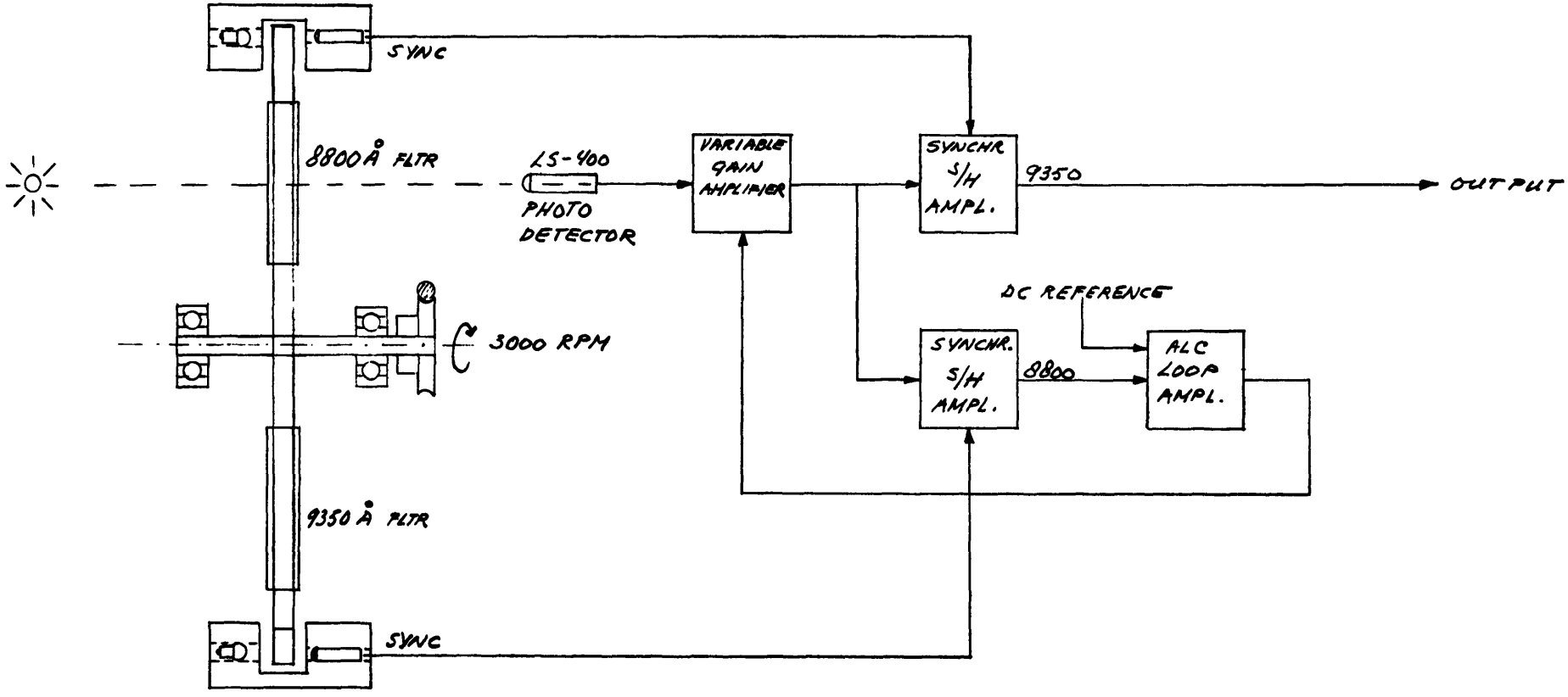

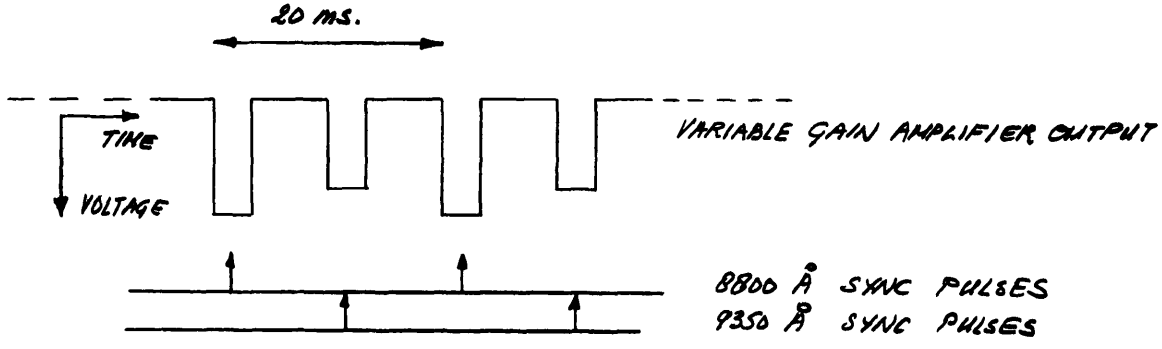

FIG 1 : HYGROMETER BLOCK DIAGRAM AND TIMING

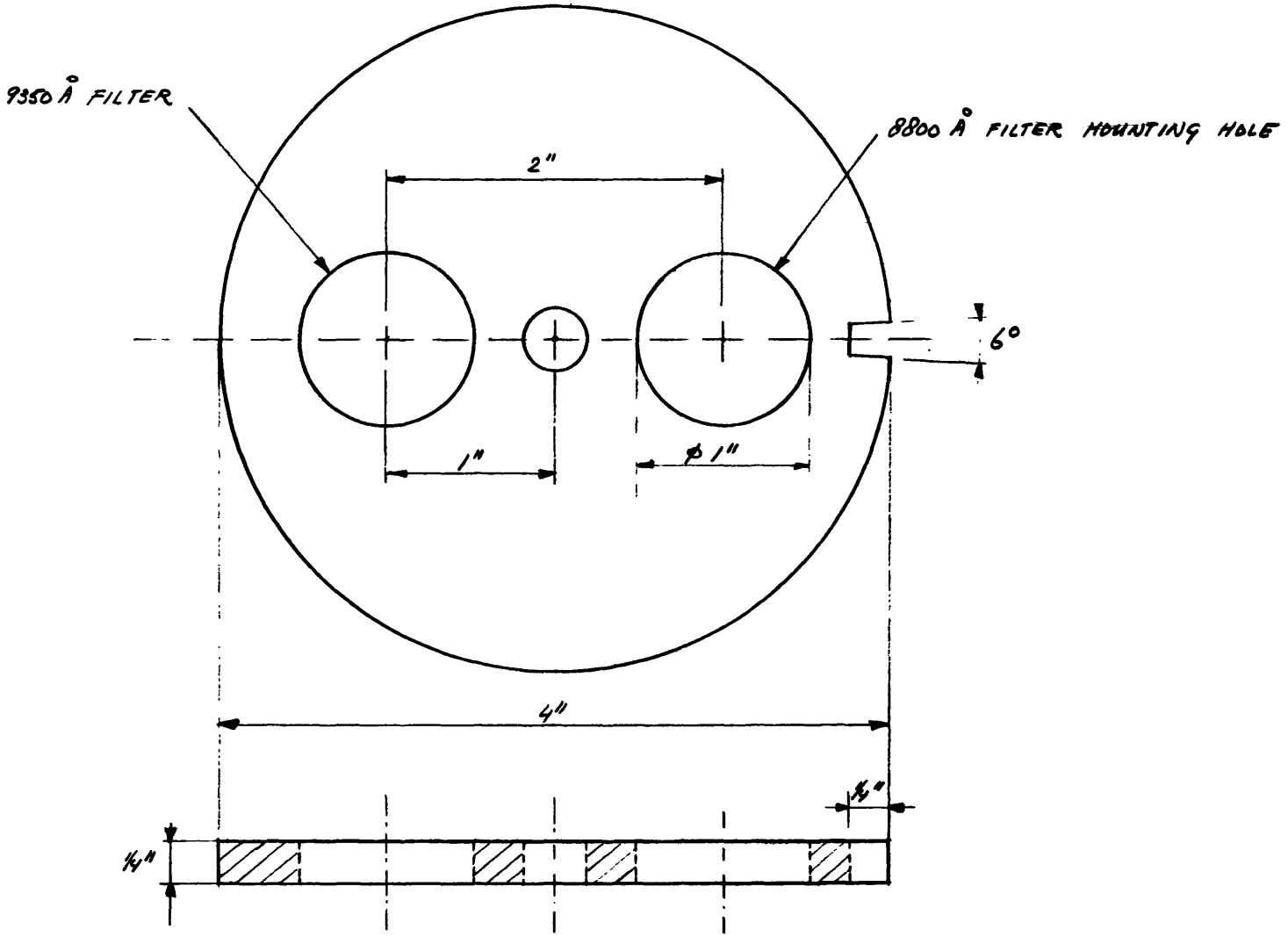

FIG. 2 : HYGROMETER FILTER WHEEL DIMENSIONS

LS-400 Ratings:

Power dissipation	50mW	
Maximum operating temperature	125°C	
Forward breakdown	8V @ 100μA	
Reverse breakdown	50V @ 100μA	
Dark current @ 30V	10nA @ 30V	
Rise time	1.5μs	at 1KΩ impedance
Fall time	15μs	at 1KΩ impedance

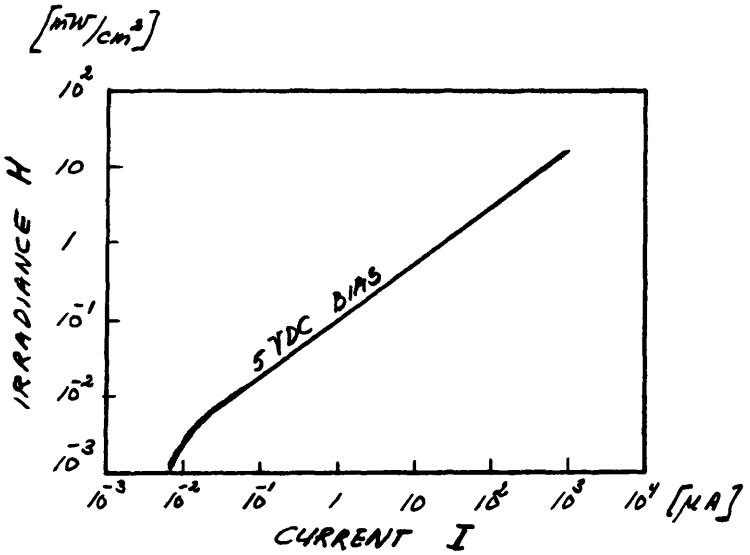

LS-400 LIGHT CURRENT VS IRRADIANCE

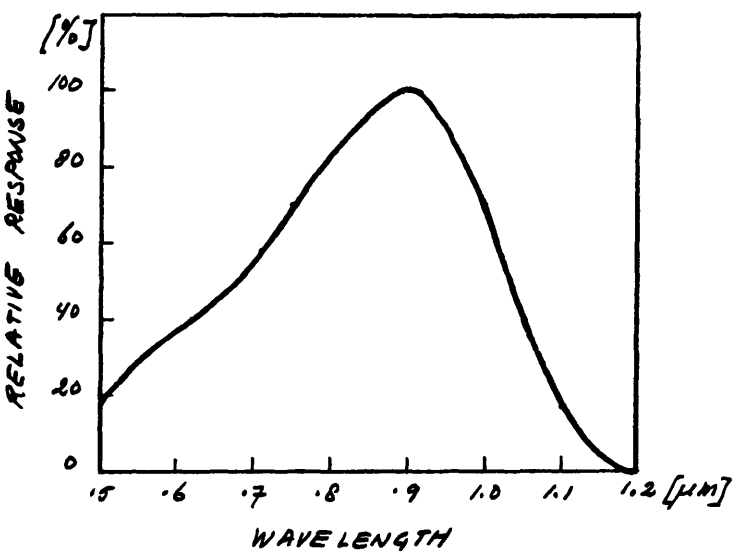

LS-400 SPECTRAL RESPONSE CURVE

FIG. 3 PERTINENT LS-400 INFORMATION

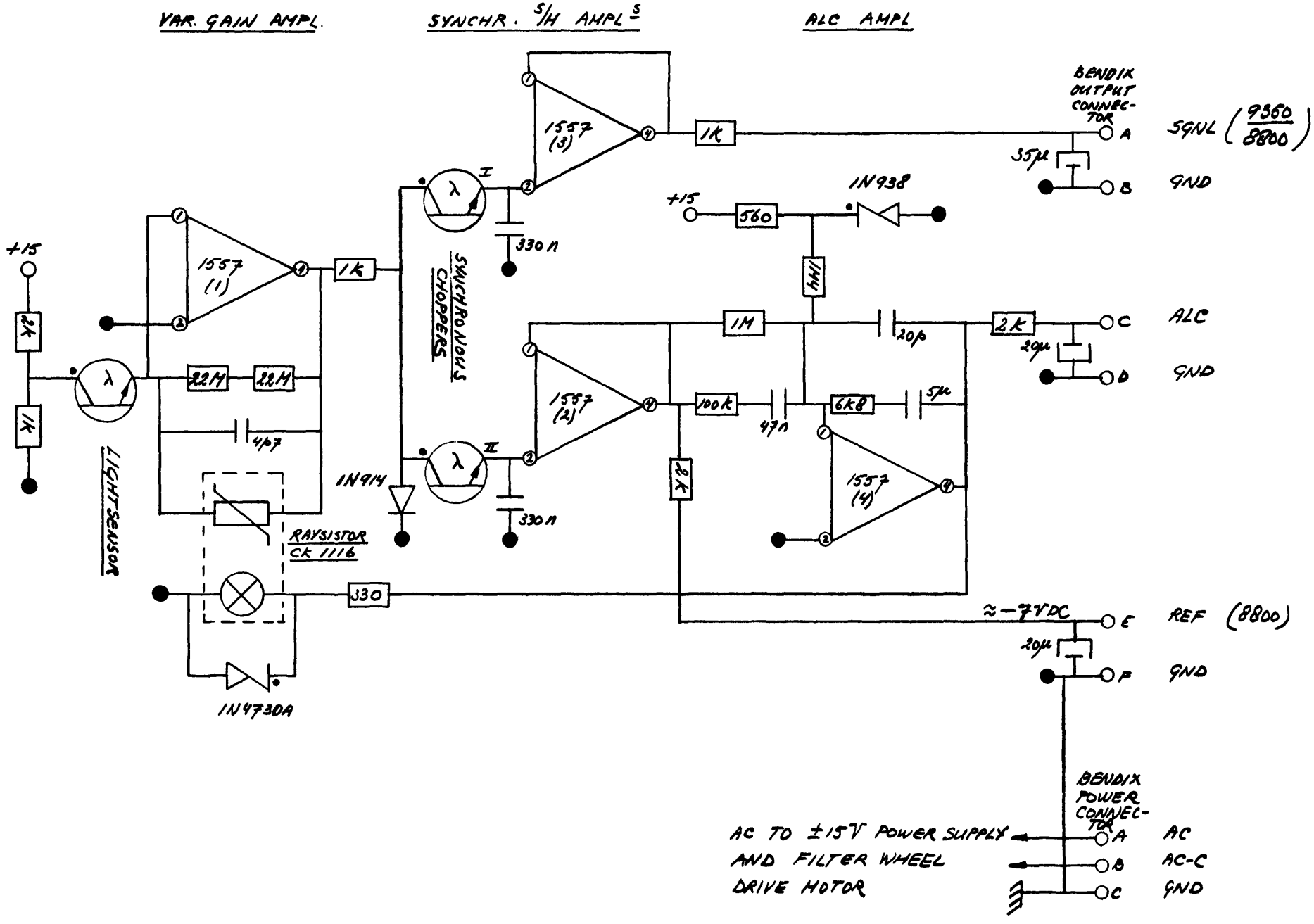

FIG. 4: HYGROMETER ELECTRONICS CIRCUIT DIAGRAM

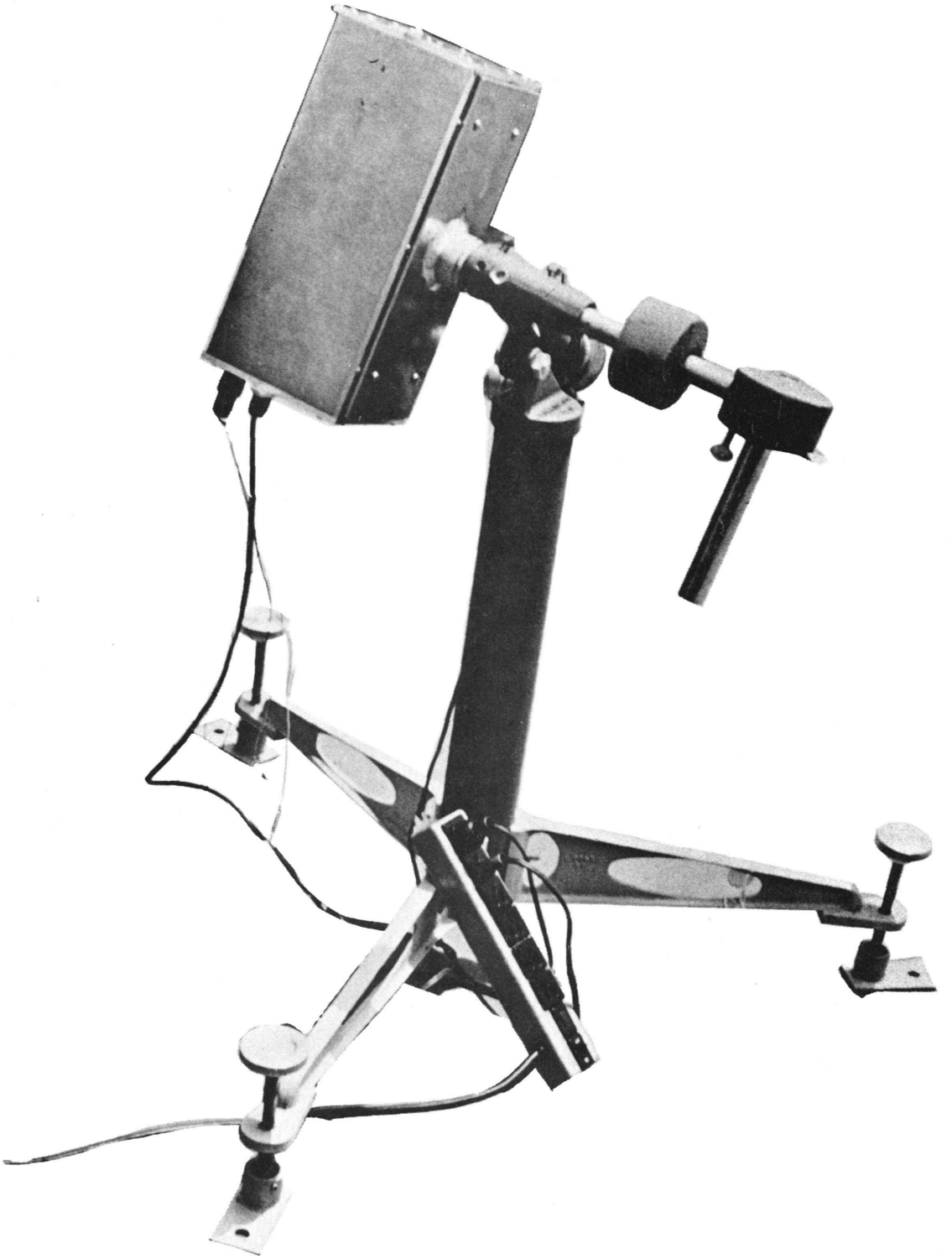

Fig. 5

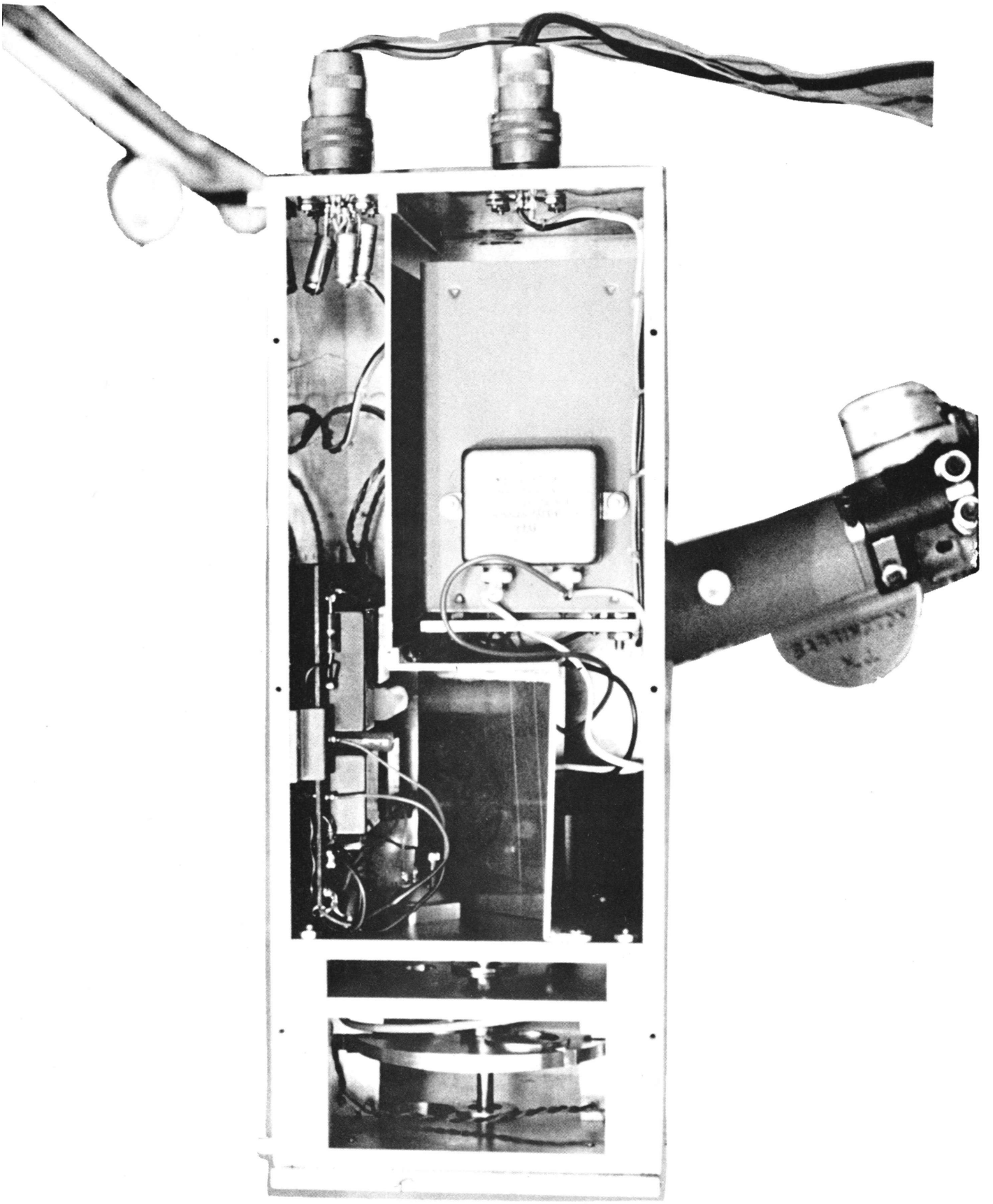

Fig. 6

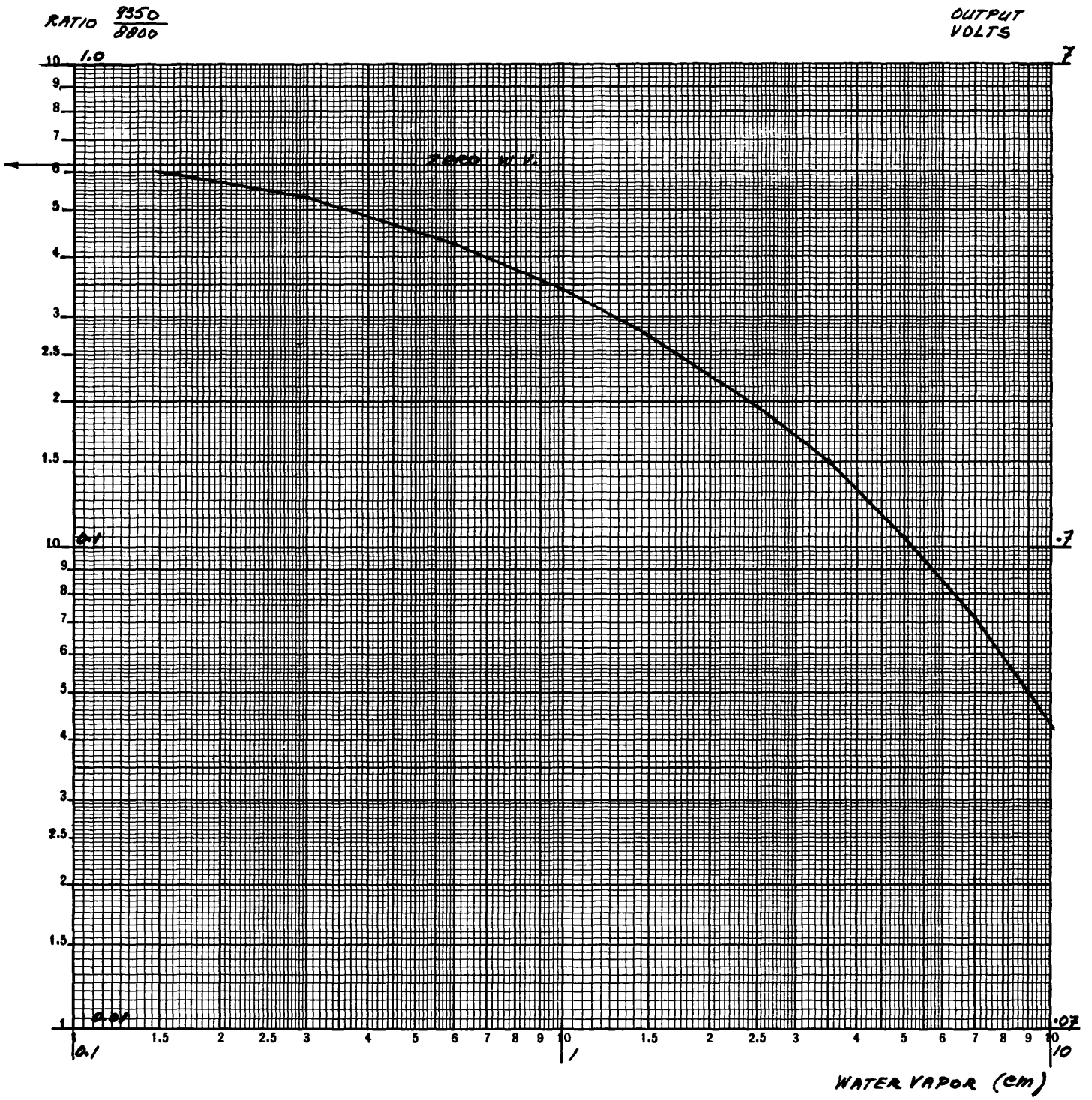

FIG. 7 HYGROMETER CALIBRATION CURVE

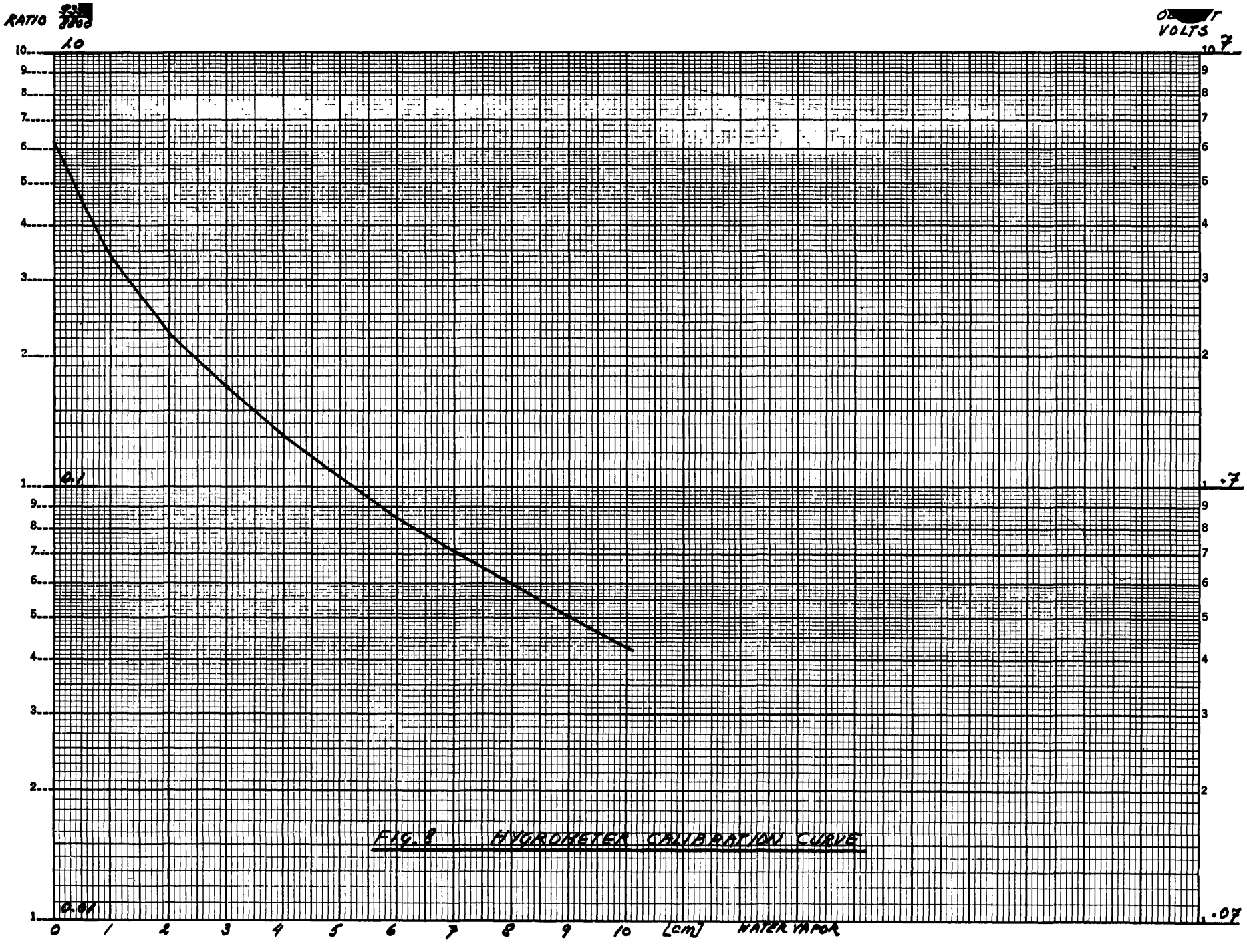

FIG. 8 HYGROMETER CALIBRATION CURVE

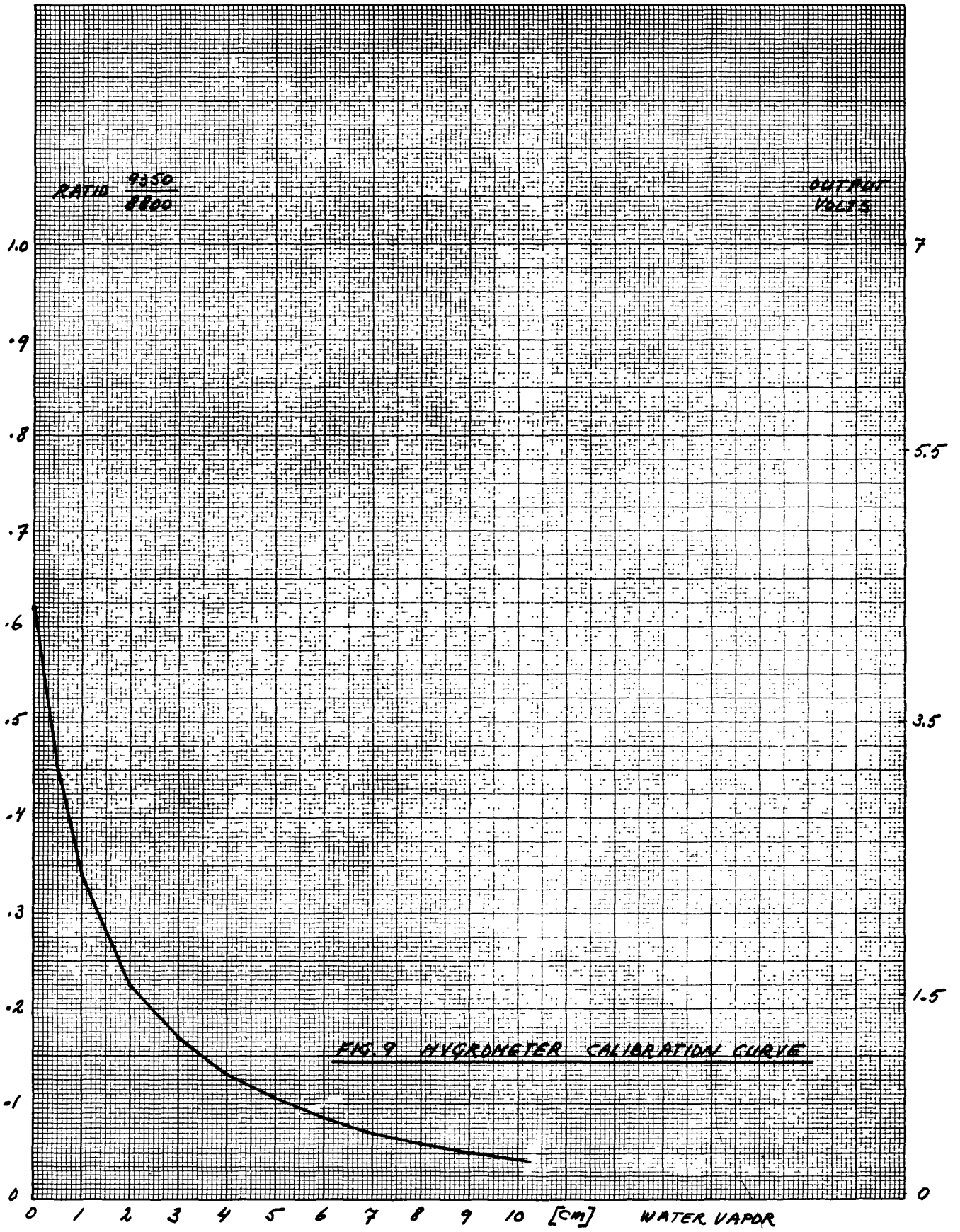

FIG. 9 HYGROMETER CALIBRATION CURVE

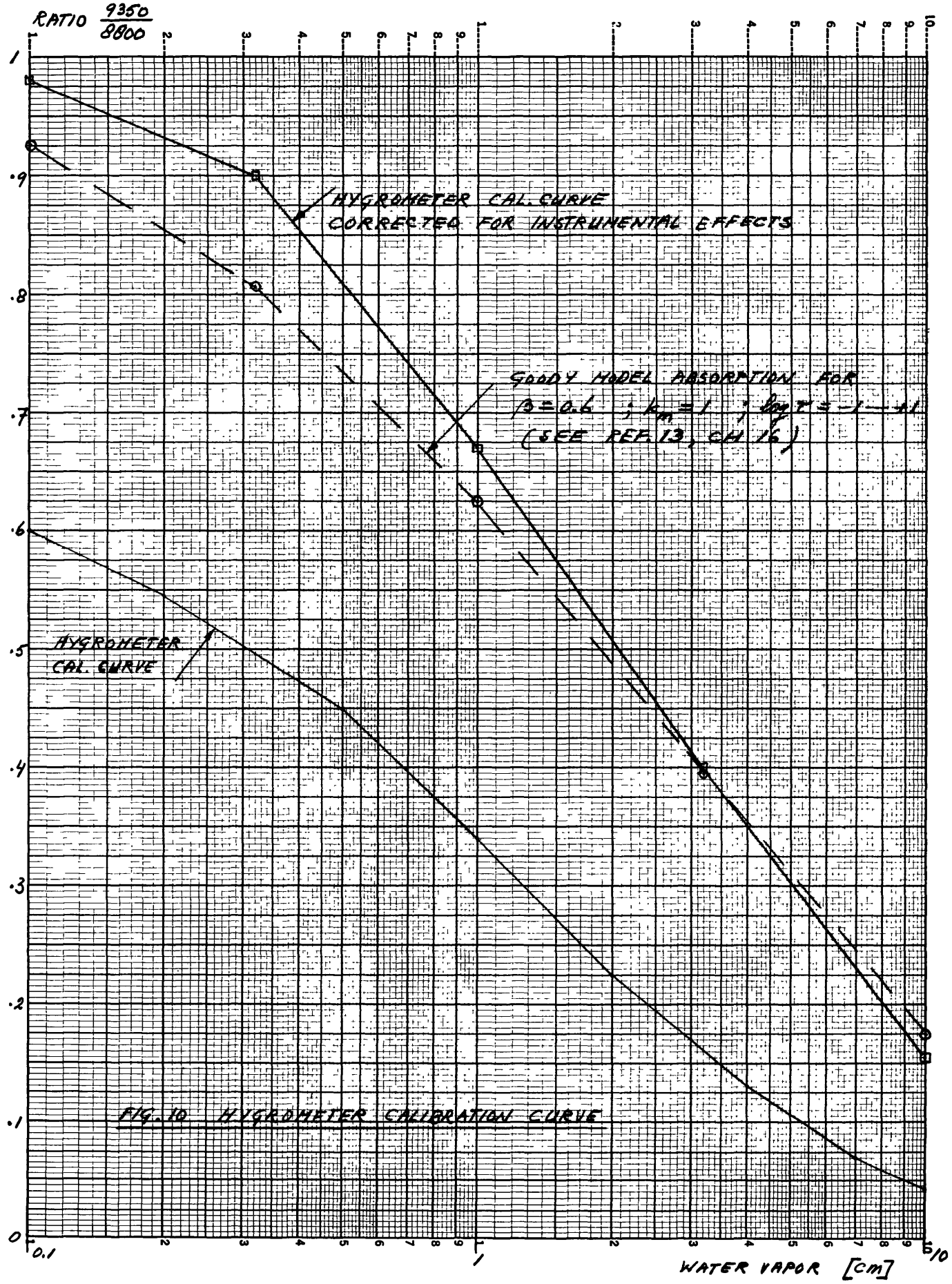

FIG. 10 HYGROMETER CALIBRATION CURVE

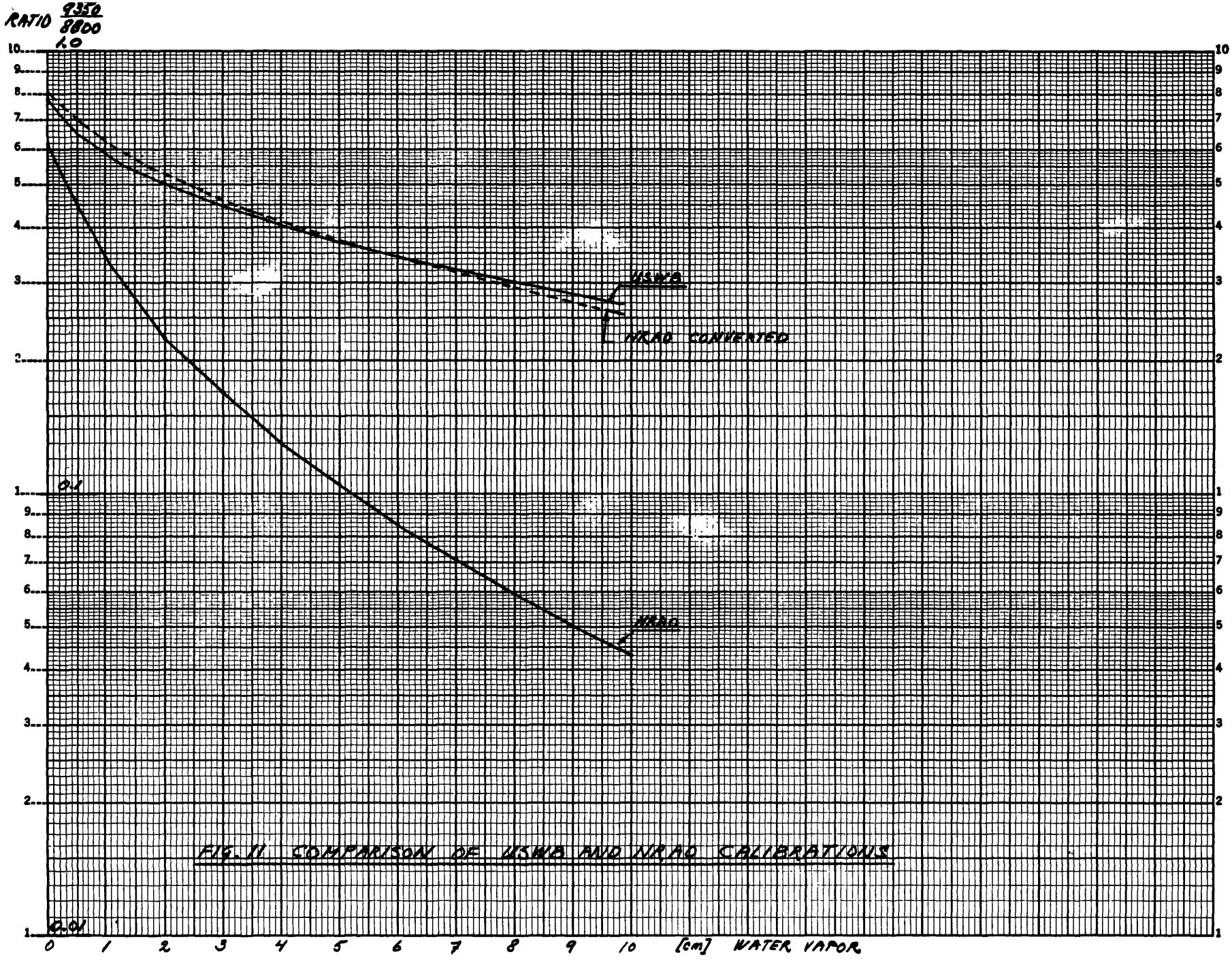

FIG. II COMPARISON OF USWB AND NRAO CALIBRATIONS

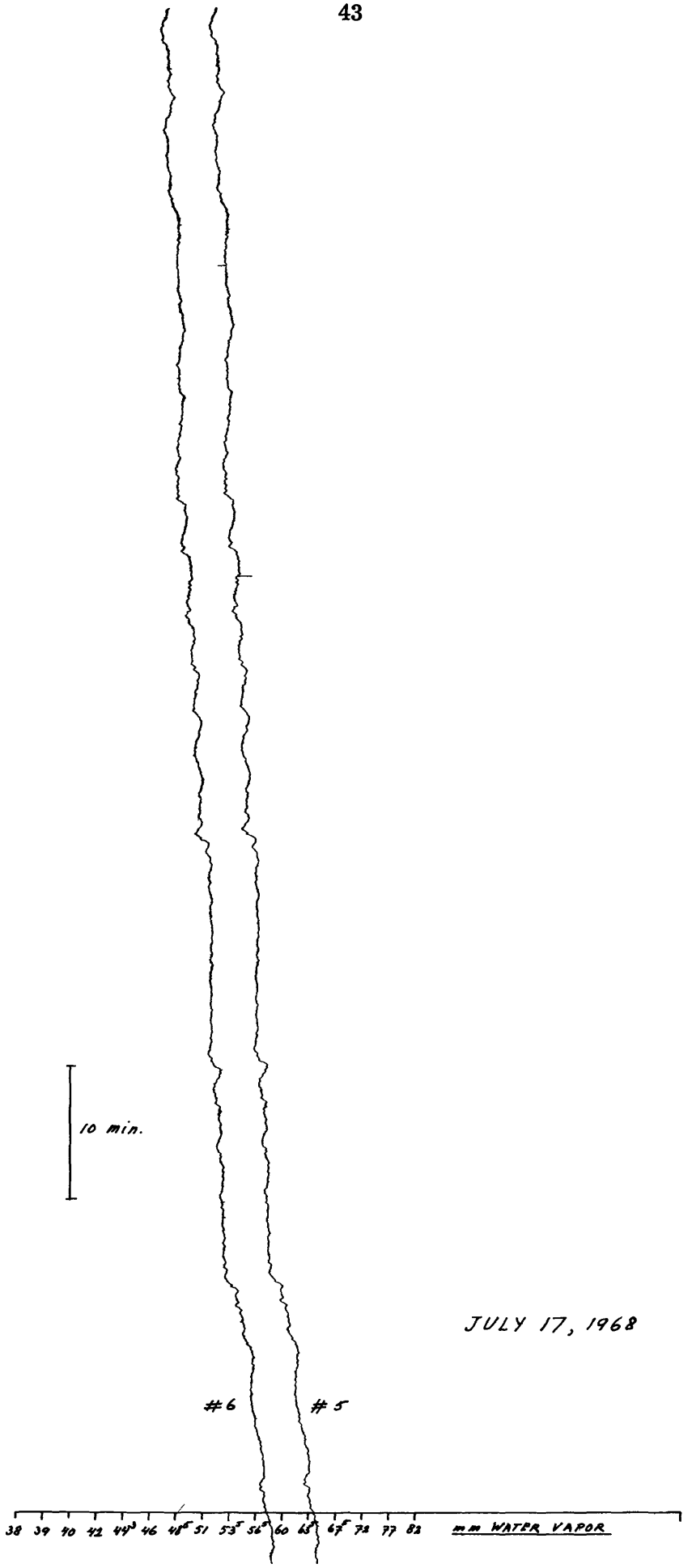
10 min.
JULY 17, 1968
#6
#5
38 39 40 42 44 46 48 51 53 56 60 65 67 72 77 82
mm WATER VAPOR

FIG. 12.

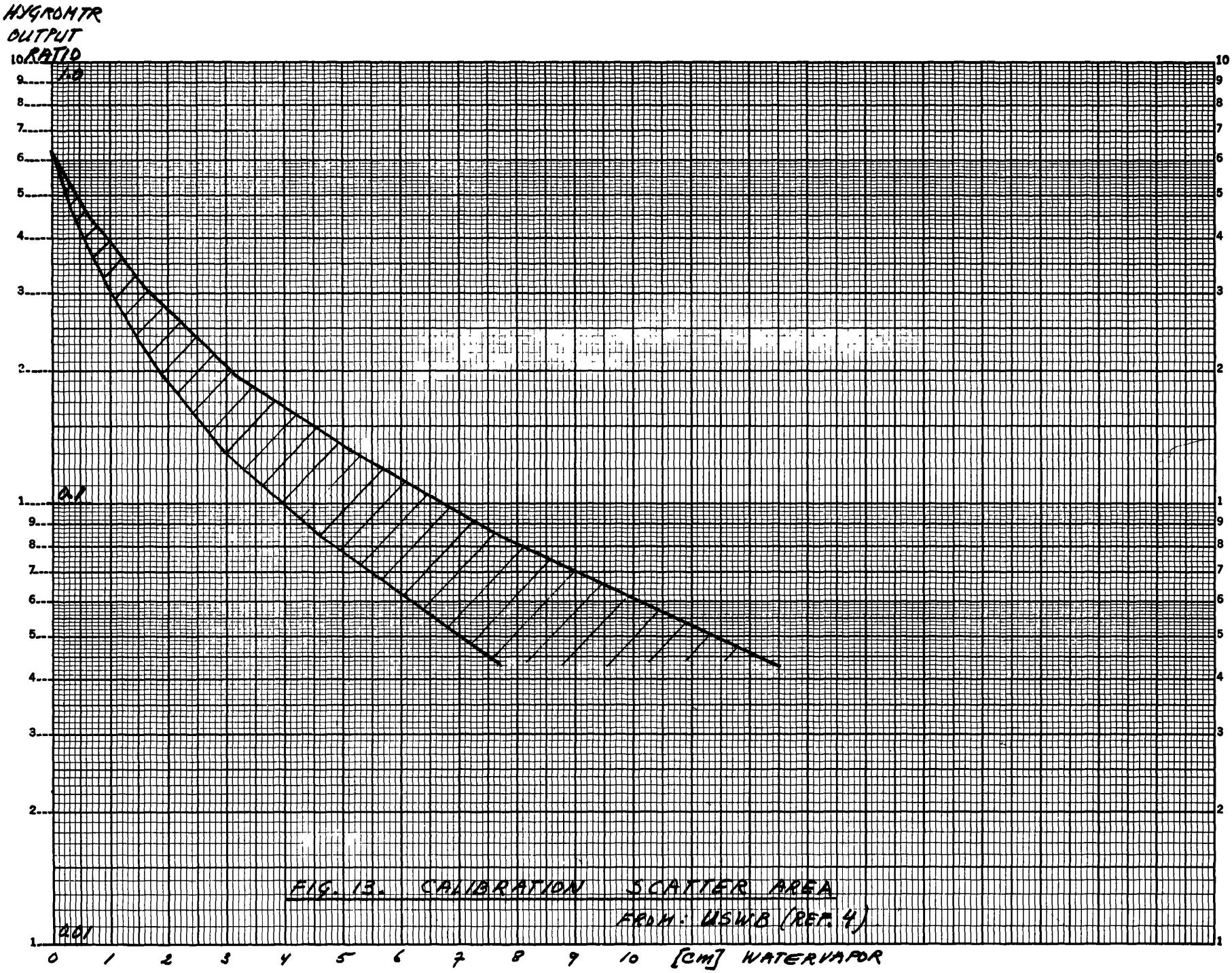

FIG. 13. CALIBRATION SCATTER AREA
FROM: USWB (REF. 4)

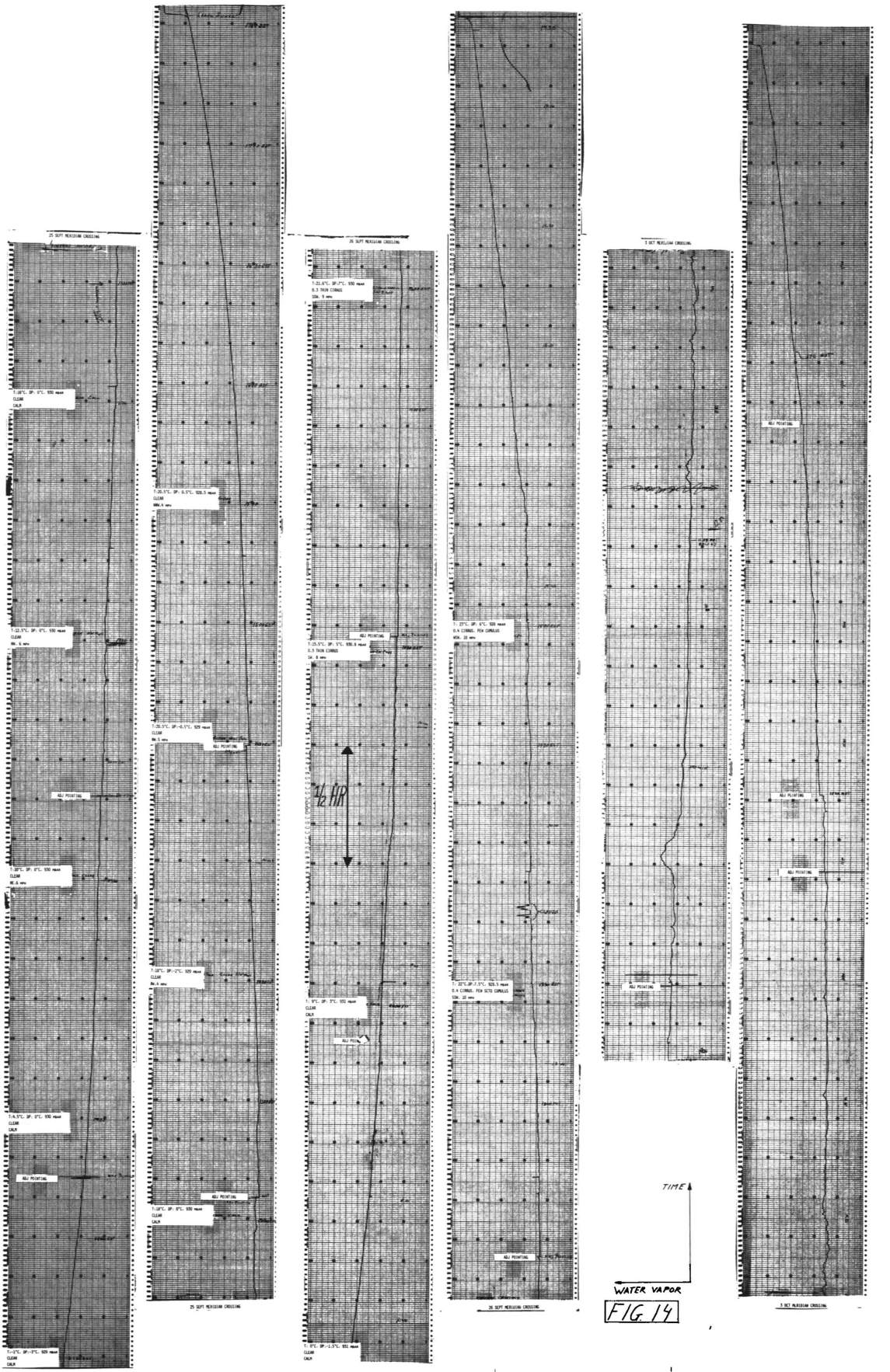

FIG. 14

25 IX 1967

26 IX 1967

3 X 1967

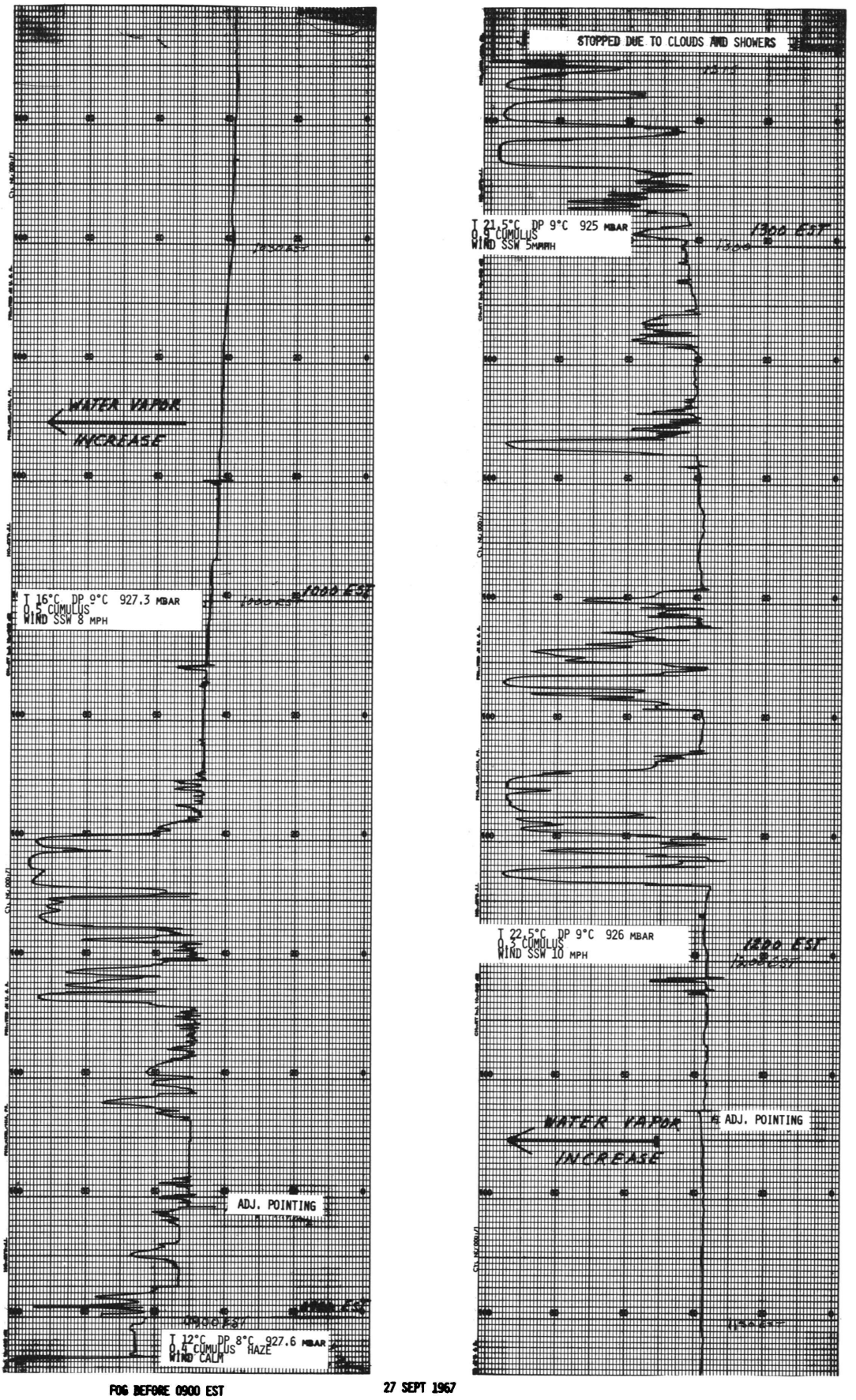

FOG BEFORE 0900 EST

27 SEPT 1967

FIG. 15

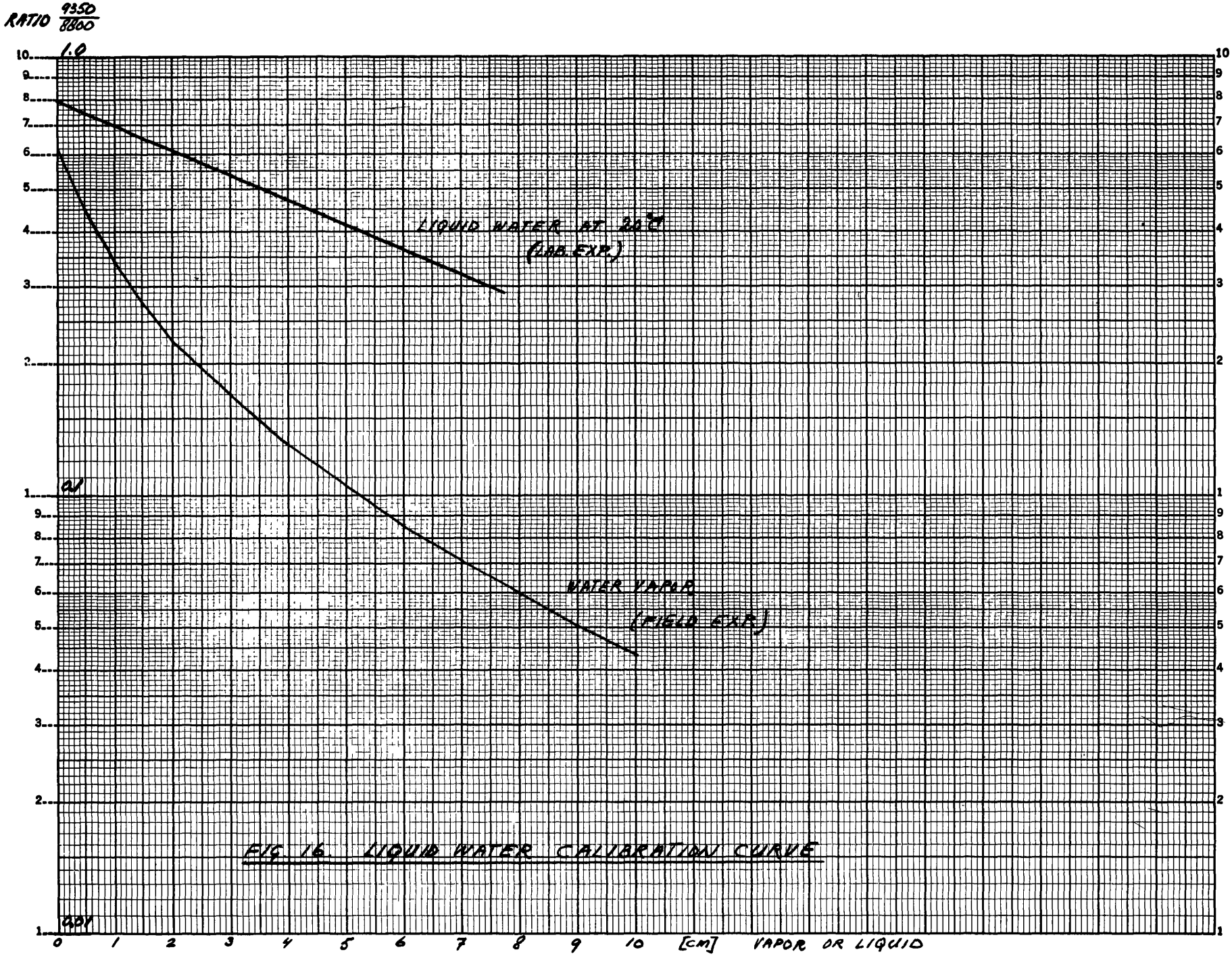

FIG 16 LIQUID WATER CALIBRATION CURVE

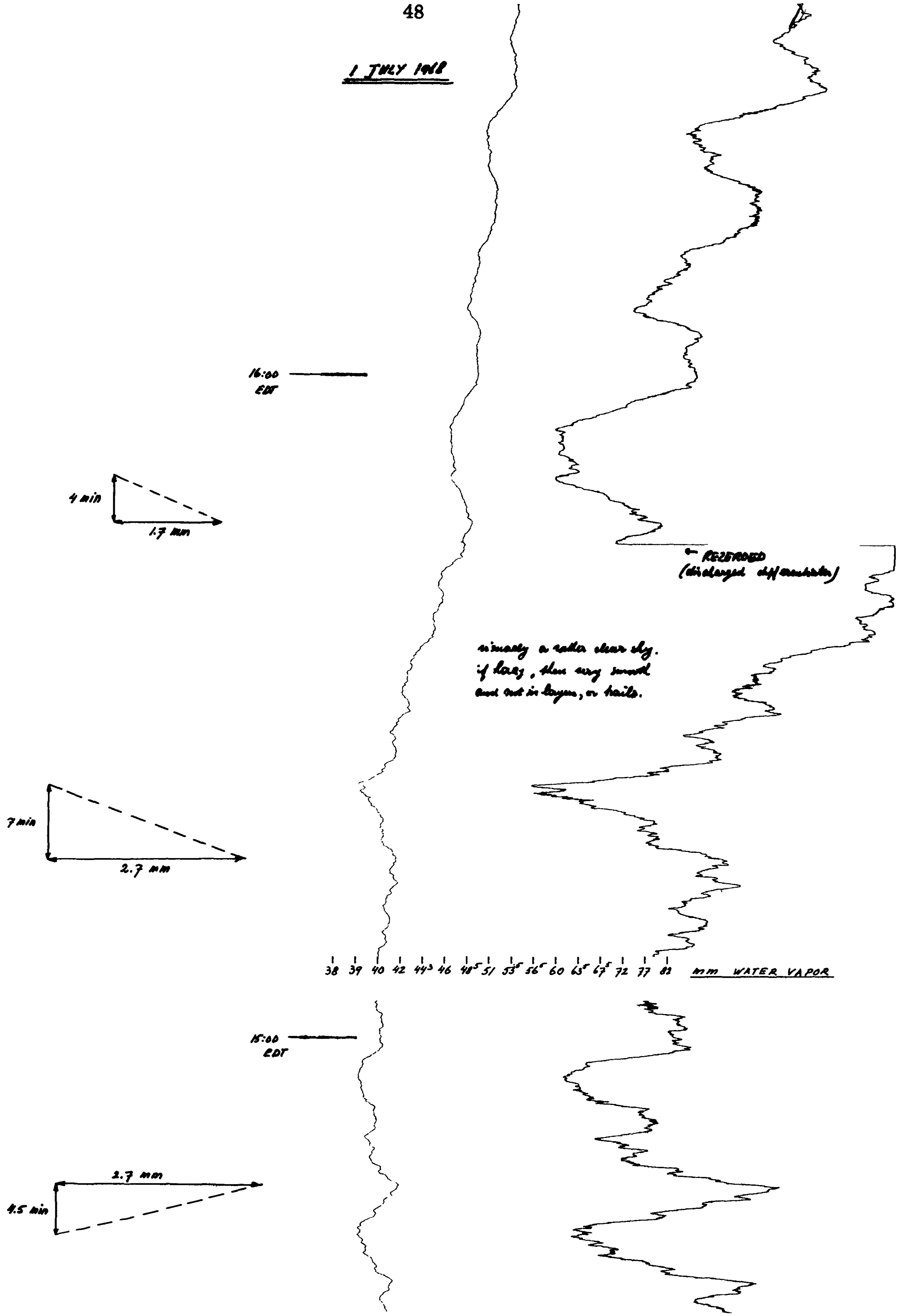
1 JULY 1968
16:00 EDT
4 min
1.7 mm
REZEROED
7 min
2.7 mm
38 39 40 42 44^3 46 48^5 51 53^5 56^5 60 65^5 67^5 72 77 82
mm WATER VAPOR
15:00 EDT
2.7 mm
4.5 min

FIG. 17

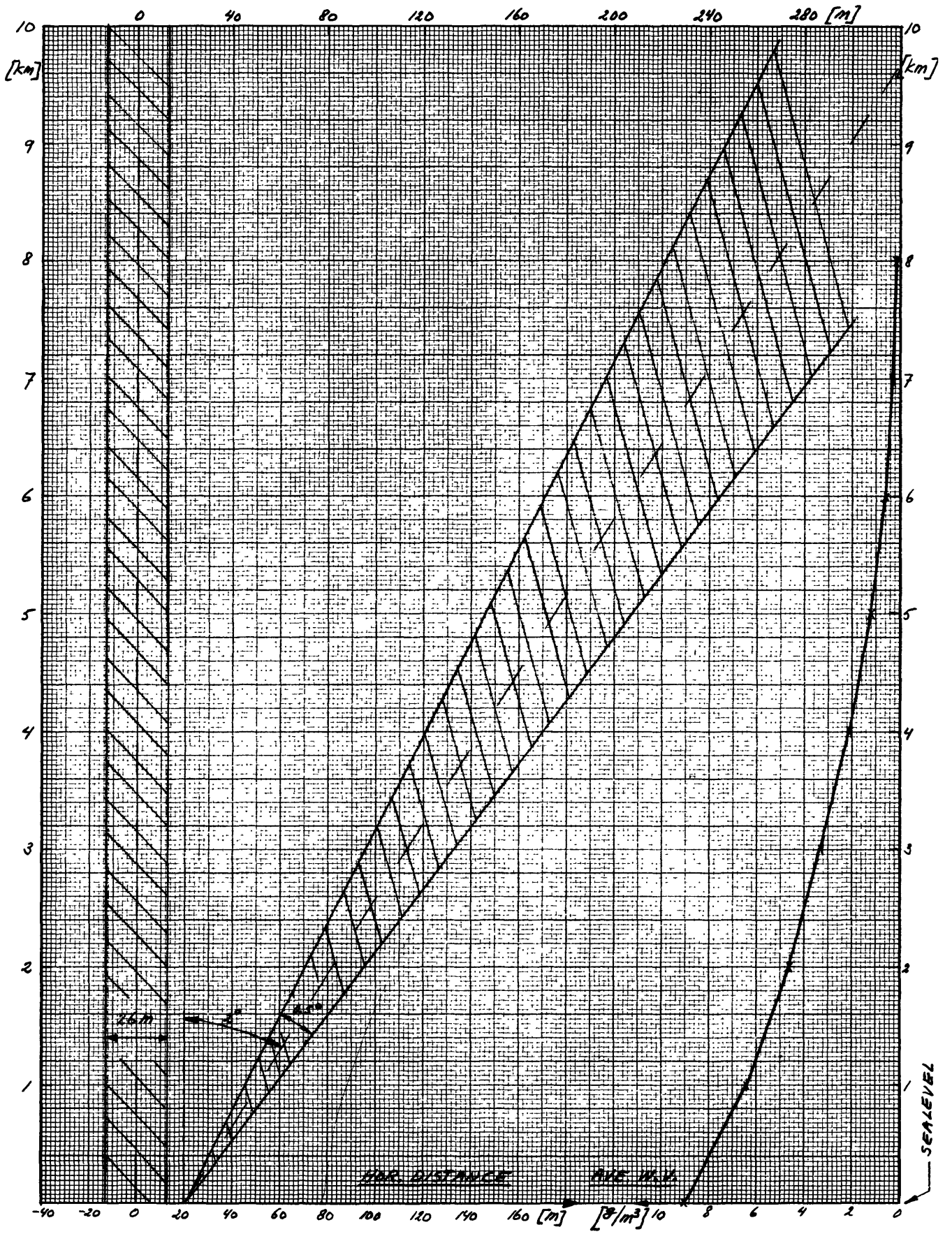

FIG. 18 INTERFEROMETER — HYGROMETER BEAM COMPARISON

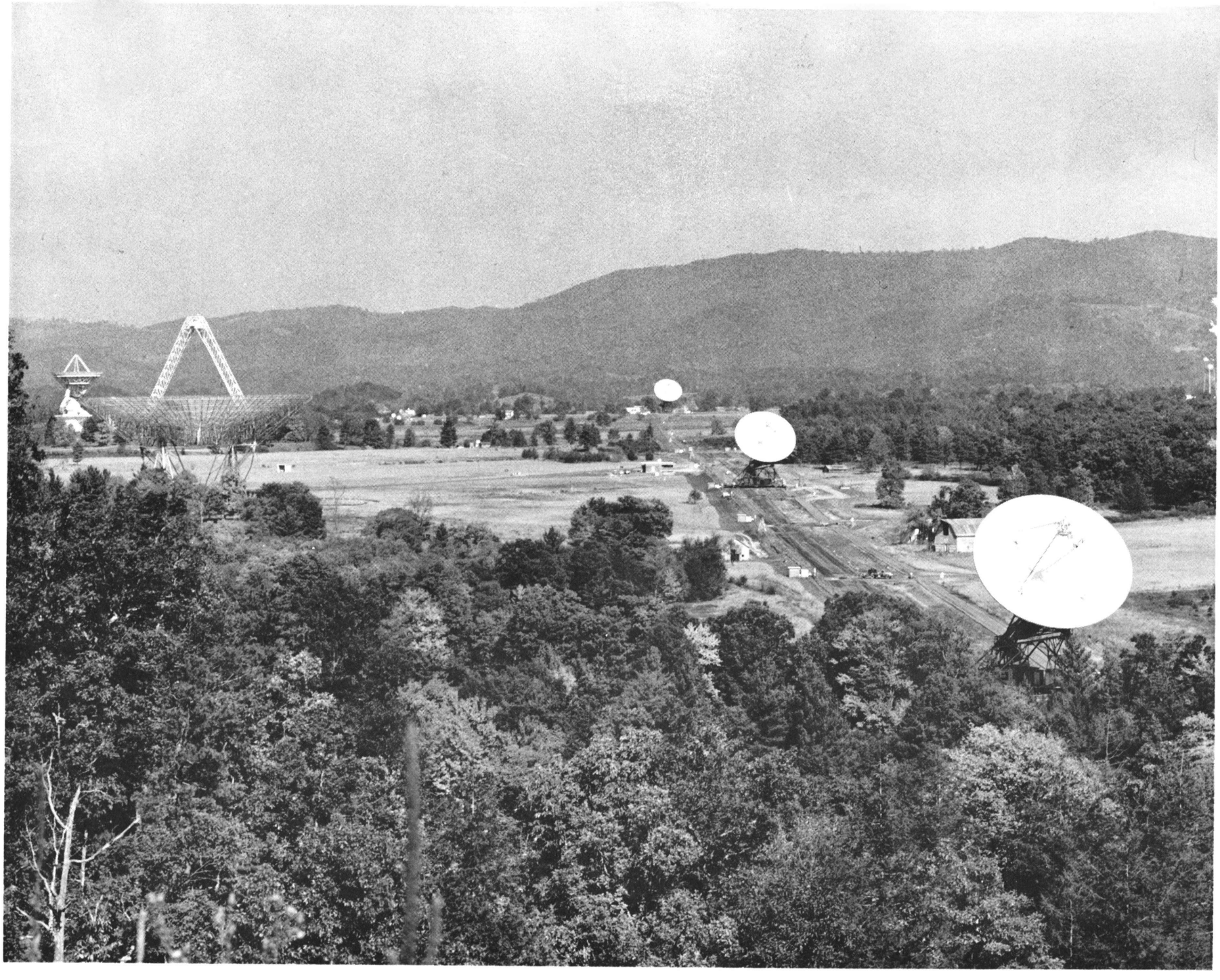

Fig. 19

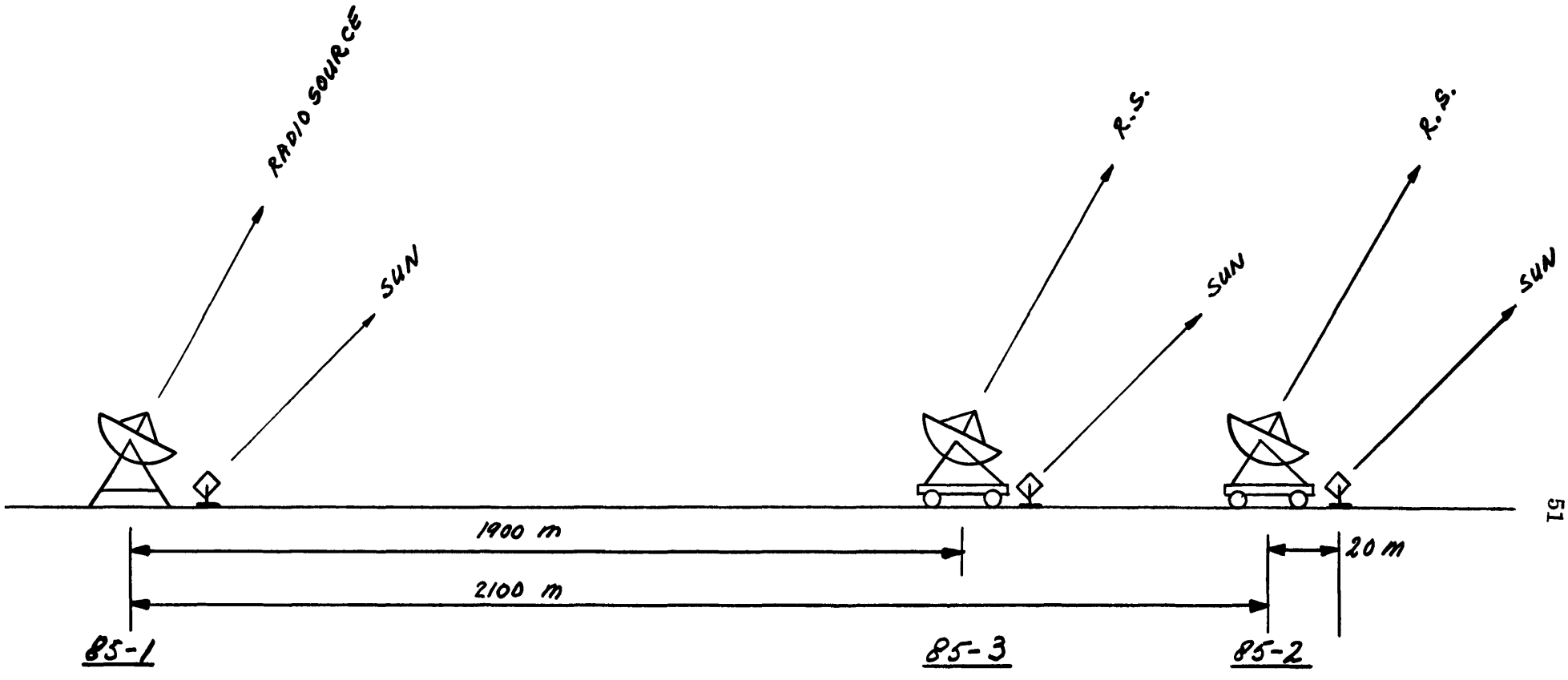

FIG. 20 : LAYOUT SKETCH OF NEAR-OCCULTATION EXPERIMENTS

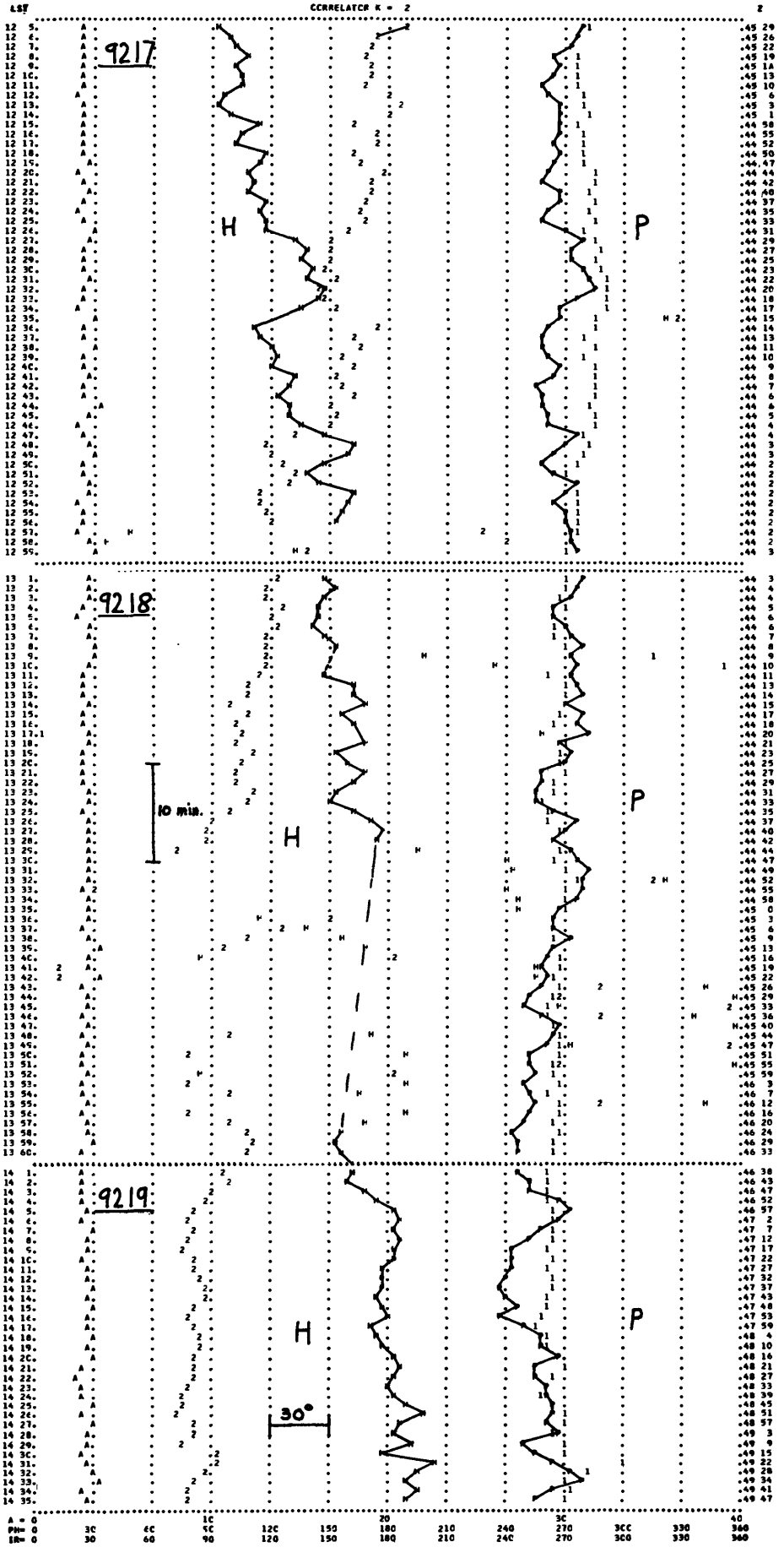

FIG. 21

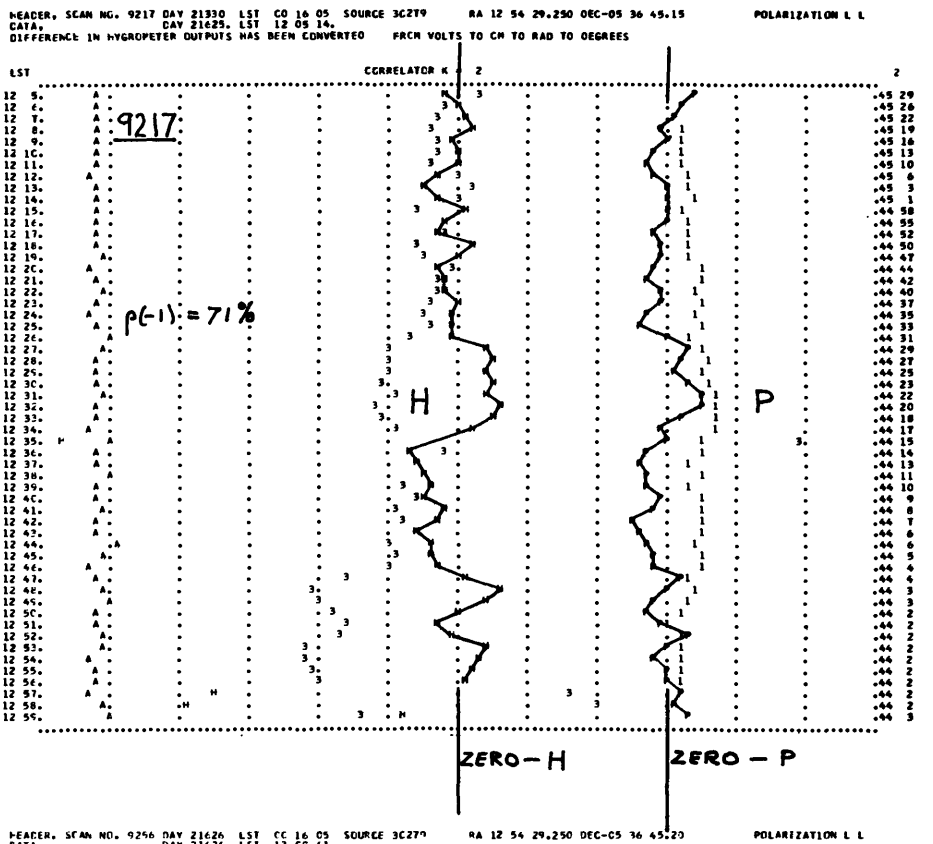
HEADER, SCAN NO. 9217 DAY 21330 LST 00 16 05 SOURCE 3C279 RA 12 54 29.250 DEC-05 36 45.15 POLARIZATION L L
DATA, DAY 21625. LST 12 05 14.
DIFFERENCE IN HYGROPETER OUTPUTS HAS BEEN CONVERTED FROM VOLTS TO CM TO RAD TO DEGREES
LST
CORRELATOR K = 2
9217
p(-1) = 71%
H
P
ZERO – H
ZERO – P
HEADER, SCAN NO. 9256 DAY 21626 LST 00 16 05 SOURCE 3C279 RA 12 54 29.250 DEC-05 36 45.20 POLARIZATION L L
DATA, DAY 21626. LST 13 00 41.
DIFFERENCE IN HYGROMETER OUTPUTS HAS BEEN CONVERTED FROM VOLTS TO CM TO RAD TO DEGREES
LST
CORRELATOR K = 2
9256
p(-1) = 68%
10 min.
H
30°
P
0 -(H)
0 -(P)

FIG 22

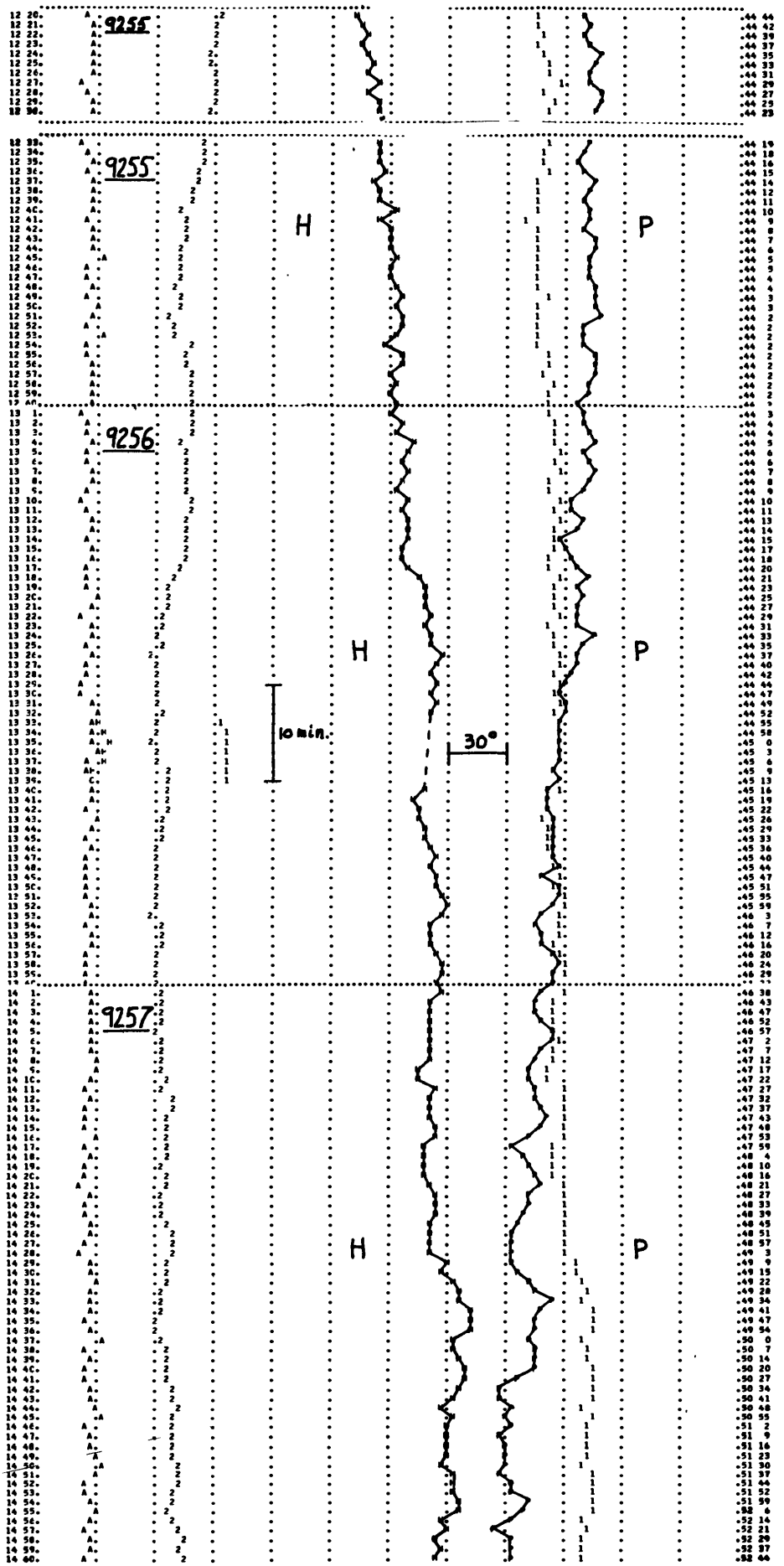

FIG 23

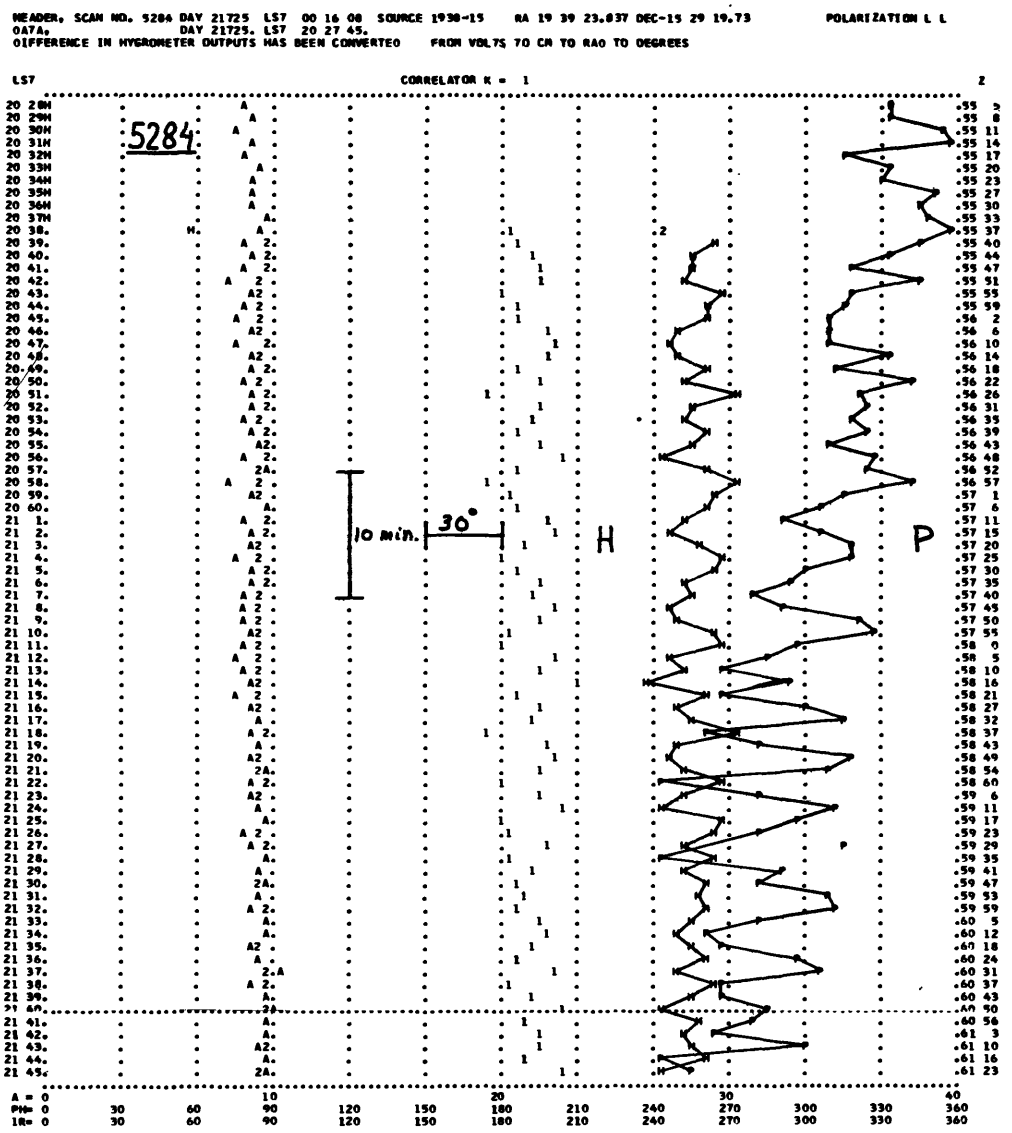
HEADER, SCAN NO. 5284 DAY 21725 LST 00 16 08 SOURCE 1930-15 RA 19 39 23.837 DEC-15 29 19.73 POLARIZATION L L
OA7A, DAY 21725, LST 20 27 45.
DIFFERENCE IN HYGROMETER OUTPUTS HAS BEEN CONVERTED FROM VOLTS TO CM TO RAD TO DEGREES
LST
CORRELATOR K = 1
Z
5284
10 min.
30°
H
P

FIG. 24